Journal of Vacuum Science and Technology B

REVIEW ARTICLE | APRIL 19 2023

Radiation damage in GaN/AlGaN and SiC electronic and photonic devices

Special Collection: Honoring Dr. Gary McGuire's Research and Leadership as Editor of the Journal of Vacuum Science & Technology for Three Decades

S. J. Pearton ; Xinyi Xia ; Fan Ren ; Md Abu Jafar Rasel ; Sergei Stepanoff ; Nahid Al-Mamun ; Aman Haque ; Douglas E. Wolfe

J. Vac. Sci. Technol. B 41, 030802 (2023)
https://doi.org/10.1116/6.0002628

07 April 2024 10:54:22

JVST B
Journal of Vacuum Science & Technology B

REVIEW

avs.scitation.org/journal/jvb

Radiation damage in GaN/AlGaN and SiC electronic and photonic devices

Cite as: J. Vac. Sci. Technol. B **41**, 030802 (2023); doi: 10.1116/6.0002628
Submitted: 1 March 2023 · Accepted: 6 April 2023 ·
Published Online: 19 April 2023

S. J. Pearton,[1,a)] Xinyi Xia,[2] Fan Ren,[2] Md Abu Jafar Rasel,[3] Sergei Stepanoff,[4] Nahid Al-Mamun,[3] Aman Haque,[3] and Douglas E. Wolfe[4]

AFFILIATIONS

[1]Department of Materials Science and Engineering, University of Florida, Gainesville, Florida 32606
[2]Department of Chemical Engineering, University of Florida, Gainesville, Florida 32606
[3]Department of Mechanical Engineering, Penn State University, University Park, Pennsylvania 16802
[4]Department of Materials Science and Engineering, Penn State University, University Park, Pennsylvania 16802

Note: This paper is a part of the Special Topic Collection Special Topic Collection Honoring Dr. Gary McGuire's Research and Leadership as the Editor of the Journal of Vacuum Science & Technology for Three Decades.
[a)]**Electronic mail:** spear@mse.ufl.edu

07 April 2024 10:54:22

ABSTRACT

The wide bandgap semiconductors SiC and GaN are commercialized for power electronics and for visible to UV light-emitting diodes in the case of the GaN/InGaN/AlGaN materials system. For power electronics applications, SiC MOSFETs (metal–oxide–semiconductor field effect transistors) and rectifiers and GaN/AlGaN HEMTs and vertical rectifiers provide more efficient switching at high-power levels than do Si devices and are now being used in electric vehicles and their charging infrastructure. These devices also have applications in more electric aircraft and space missions where high temperatures and extreme environments are involved. In this review, their inherent radiation hardness, defined as the tolerance to total doses, is compared to Si devices. This is higher for the wide bandgap semiconductors, due in part to their larger threshold energies for creating defects (atomic bond strength) and more importantly due to their high rates of defect recombination. However, it is now increasingly recognized that heavy-ion-induced catastrophic single-event burnout in SiC and GaN power devices commonly occurs at voltages ~50% of the rated values. The onset of ion-induced leakage occurs above critical power dissipation within the epitaxial regions at high linear energy transfer rates and high applied biases. The amount of power dissipated along the ion track determines the extent of the leakage current degradation. The net result is the carriers produced along the ion track undergo impact ionization and thermal runaway. Light-emitting devices do not suffer from this mechanism since they are forward-biased. Strain has also recently been identified as a parameter that affects radiation susceptibility of the wide bandgap devices.

Published under an exclusive license by the AVS. https://doi.org/10.1116/6.0002628

I. INTRODUCTION

While Si high-voltage devices are still the most used components for power conversion, they have insufficient breakdown capabilities for many applications, such as power switching for the electricity grid.[1–7] Since the typical voltage range for power transmission is 100 kV to 1.2 MV, this would require the serial stacking of large numbers of Si devices to achieve such high voltages. Even the voltages required for power distribution systems are in the range of 4–100 kV, well beyond the capability of individual Si devices. As a result of their larger bandgaps >3 eV compared to 1.1 eV for Si, these so-called wide bandgap (WBG) semiconductors, SiC and GaN, can achieve superior high-power switching performance than Si with much lower switching losses.[1–4,6]

Both of these semiconductors have been commercialized for high-power, high-temperature electronics applications. They have significantly improved energy efficiency in power switching applications relative to Si devices.[1–7] They can also operate at higher temperatures. As an example, SiC devices and small-scale circuits have been shown to be capable of operation to 500 °C, as part of the control systems needed for space exploration missions to Venus.[8–11] These WBG power switches have begun to replace Si in applications, such as electric vehicle power trains and charging

Published under an exclusive license by the AVS

systems because of their advantages in terms of higher current density, faster switching, near-zero reverse recovery time, lower drain-source on-resistance, improved temperature tolerance, and smaller form factor.[1–11] The high-temperature capability is exploited in high-temperature or harsh environments. Some examples include data logging when drilling during geothermal energy collection, turbines, and sensing of gases in industrial environments. SiC also has been suggested as a potential host for quantum qbits for quantum computers.[12]

Some additional emerging markets for wide bandgap electronics include 5G infrastructure, renewable energy generation, and data centers, where energy savings with more efficient electronics can be enormous.[1–11] In electric vehicles, the currently used 8 kHz Si power transistors in DC-to-AC traction inverters and on-board chargers are being replaced with 600–1200 V SiC. To increase charging speed of battery packs in electric vehicles, the current 400–600 V systems are expected to transition to 800–1200 V.[1–7] At voltages beyond the transportation applications, SiC devices with >1200 V capabilities are expected to be used in for high-power solar farms and large three-phase grid converters.[1–11] GaN FETs are typically 600–900 V devices for high-density converters with power >10 kW for consumer, server, telecom, and industrial power supplies grid converters.[6,7] The two technologies overlap at powers below 10 kW.[5–7]

Another application for these SiC and GaN devices is in space-based satellite and defense systems not only for their high-temperature capability but because they are more radiation-hard to displacement damage and total ionizing dose effects than Si.[13–16]

II. MATERIALS PROPERTIES OF SiC AND GaN

SiC has several crystal structures or polytypes,[4,5] with the most common being 4H-SiC, 6H-SiC, and 3C-SiC. Both the 4H- and 6H-SiC polytypes have hexagonal crystal structures, while 3C-SiC has a zinc-blende crystal structure. Table I compares the material properties of 4H-SiC with GaN and AlN, the two endpoints of the AlGaN materials system. There are some noteworthy points from this table, apart from the usual aspect of a wide bandgap for high voltage and temperature operation. The wide bandgap provides a transparent window range from the visible to mid-infrared wavelengths. This contrasts with Si, which is transparent only in the infrared.[6] The thermal conductivity of SiC is second to diamond among dielectrics. SiC also has large Young's modulus, making it attractive for high frequency micromechanical devices. Divacancy point defects also form in SiC, With their relatively long spin coherence times, they are possible options in optical systems based on quantum effects.[12] Figure 1 shows a spider diagram, which compares the device attributes best suited to each material. Compared to Si, these are clearly high voltage, high-temperature, high frequency applications for SiC and GaN.

With all the progress in crystal growth, device processing, packaging, and thermal management, one of the only real disadvantages is still that the oxide/SiC interface has high defect densities compared to SiO_2 or other dielectrics on Si. These defects, such as dangling bonds and free and complexed carbon, limits the performance and reliability of SiC power MOSFETs by degrading the channel mobility and device reliability.

TABLE I. Summary of properties for SiC, GaN, and AlN. The various figures of merit for each material are normalized to Si (Refs. 4–7).

Parameter	AlN	4H-SiC	GaN
Bandgap (eV)	6.0	3.25	3.4
Dielectric constant	9.8	9.7	9
Breakdown field (MV cm^{-1})	15	2.5	3.3
Electron mobility (cm^2/V s)	400	1000	1250
m_e/m_o	0.31	0.39	0.20
m_h/m_o	0.42	0.82	1.00
Saturation velocity (10^7 cm/s)	1.2	2	2.5
Thermal conductivity (W/mK)	320	490	230
Bulk modulus (GPa)	190	700	290
Moh's hardness	7	9.3	∼6
Surface hardness (GPa)	14	30	12
Density (g cm^{-3})	3.26	3.2	6.1
Doping capability	N high P low	N med P high	N high P low
E_D (meV)	90	60	25
E_A (meV)	500	250	170
Substrate size (mm)	50	150	100
T_S (°C)	3000	2800	2500

For GaN, it has the advantage of two different heterostructure systems: GaN/AlGaN and GaN/InGaN. The former is used for power electronics and UV LEDs, while the latter is used for visible LEDs. Bulk GaN substrates are available but still are expensive and variable in quality; therefore, it is common to grow epitaxial layers of GaN on substrates, such as SiC, Si, or sapphire. Thick epitaxial layers are also still under development for achieving high breakdown (>20 kV) rectifiers.

07 April 2024 10:54:22

III. SUMMARY OF RADIATION EFFECTS

It is widely accepted that SiC and GaN devices have high inherent resistance to total dose radiation effects but are less robust

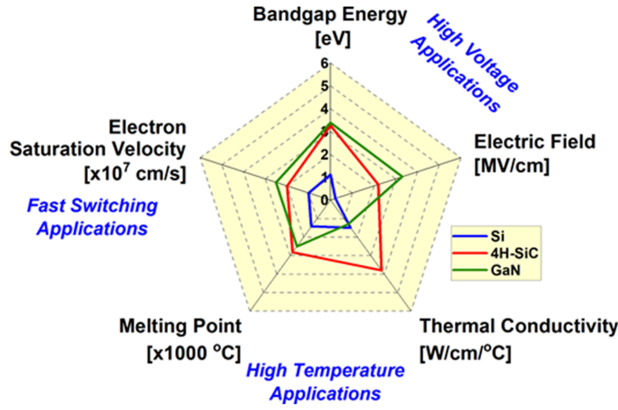

FIG. 1. Spider diagram of relative advantages of SiC and GaN over Si in device applications.

Published under an exclusive license by the AVS

against transient radiation effects.[17–37] The latter are classed under single-event effects (SEEs) and are important in space environments. In space, the radiation comes from three sources, namely, (i) solar flares, (ii) trapped protons or electrons in the Van Allen radiation belts, and (iii) galactic cosmic rays (GCRs). For solar flares and the trapped radiation, protons have energies from 1 keV to 500 MeV, while the electron energy ranges are from 1 eV to 10 MeV.[38–45] The GCRs originate from sources outside our solar system and are predominantly protons (90%) and heavier elements spanning the periodic table but with much lower fluxes for the heavier ions. The energy range of cosmic rays reaches the TeV region, again with much lower fluxes as energy increases. In the past 40 years, there have only been 22 events with energies beyond 10^{20} eV. These are referred to as super-Greisen–Zatsepin–Kuzmin occurrences. This corresponds to a flux of one event per km^2 per century.

An important parameter is the energy required to create an electron-hole pair, E_i, in a semiconductor. The most accepted empirical relation is[46–54]

$$E_i = 2.8E_g + 0.6 \text{ eV}.$$

For GaN, this corresponds to 10.1 eV or $\sim 2.5 \times 10^{12}$ e/h pairs per rad cm^3. For 4H-SiC, the value is 9.65 eV or 2.6×10^{13} e/h pair per rad cm^3. For AlN, this corresponds to 17.4 eV or 1.45×10^{12} e/h pair per rad cm^3. In terms of relative energy deposition, the non-ionizing energy loss (NIEL) or energy that goes into displacements is about 0.1% of the total energy loss.[32–37] The vast majority goes into electronic energy loss mechanisms, such as ionization, e-h pair production, and phonon creation.

For devices, the three different radiation effects are relevant: single-event effects (SEEs), total ionizing dose (TID), and displacement damage (DD). It is common to treat SEEs separately since they result from interactions of a single energetic particle. By contrast, TID and DD are cumulative effects related to the ionizing dose and the particle fluence, respectively.[17–25] The Total Ionizing Dose (TID) is a result of ionizing radiation inducing excess charge in the dielectric layers used in MOS devices. When such an MOS device is irradiated, large numbers of e-h pairs are created in the dielectric according to the relation discussed earlier. When the oxide is under bias, the electrons that do not recombine drift to the contacts. The time scale for this is short, on the order of picoseconds. In all oxides, holes have much lower mobility than the electrons, and for positive bias during the radiation exposure, they drift to the semiconductor/dielectric interface, where some become trapped at defects.[14,16] This trapping induces a positive charge buildup in the dielectric, which screens the applied bias and alters the electric field in the semiconductor. The trapped charge is apparent as a shift of device threshold voltage. Thus, TID affects mainly devices with MOS or MIS gates. Finally, displacement damage is displacement of lattice atoms from their original substitutional positions by nuclear scattering and fission and nuclear reactions. These point defects generally create new energy levels in the bandgap, which act as carrier traps and reduce carrier mobility. These changes manifest as degradation in device dc and ac performance.

Single-Event Effects (SEEs) are due to single energetic particles. The passage of such ions may cause transient errors, which include Single-Event Upset (SEU) and Single-Event Transient (SET). They may also cause so-called hard errors. These include Single-Event Latch-up (SEL), Single-Event Gate Rupture (SEGR), and Single-Event Burnout (SEB).[31–37] Figure 2 shows a schematic of the three different types of radiation damage created in semiconductor devices.

The WBG materials are more radiation-hard than Si because of their stronger atomic bonding. This reduces the density of point defects created per unit energy of ionizing radiation. However, this is not enough to explain the empirical differences in carrier removal rates between GaN, SiC, and Si. The former two have a much higher degree of dynamic annealing that occurs during the irradiation. If one employs as a figure of comparison the carrier removal rate in these materials relative to that number in Si, then a reasonable estimate is that GaN and SiC are at least 1–2 orders of magnitude less susceptible to defect creation (displacement damage) by radiation exposure.[17–37]

In terms of the effects produced by different types of radiation, photons (gamma rays and x-rays) and neutrons primarily produce ionization effects and displacement damage, respectively. Neutrons can produce Gossick zones, which are regions of dense lattice disorder surrounded by relatively defect-free areas. This has complicated effects on devices, and the spatial location of the high damage regions within the depletion region is important. High energy photons may create displacement damage by the Compton mechanism. Neutrons can initiate nuclear reactions, which produce secondary particles, such as photons. In turn, these create ionization in the semiconductor.[13–16]

Charged particles, such as protons and alpha particles, produce both displacement and ionization damage. When

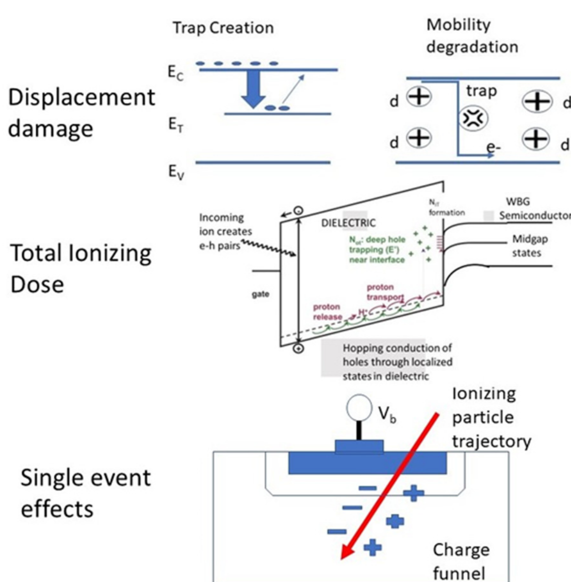

FIG. 2. Schematic of radiation effects in semiconductors.

07 April 2024 10:54:22

Published under an exclusive license by the AVS

traversing a semiconductor device, they experience Coulombic interactions with the electrons in the elements comprising the semiconductor, which reduces their energy along the ion track. For low energies in the range of keV, Coulombic collisions with the atoms in the semiconductor are the main energy loss mechanism.[53–65] In terms of relevant doses, the current defense system requirements for TID are 300 krad (Si), SEU is 10^{-10} errors/bit-day, SEFI 10^{-5} errors/chip-day, DR Upset >10^8 rad (Si)/s, and displacement damage 10^{12} n/cm^2.

The magnitude of defect production and the resultant damage accumulation depend on the relative energy lost to electronic energy loss (S_e) or nuclear energy loss (S_n).[17–39] The interplay between these can be complex, producing additive, competitive, or synergistic effects on how the damage evolves. The electronic stopping power is also known as the inelastic linear energy transfer (LET) to the semiconductor. The ionization produced by this energy loss consists of creation of e-h pairs on a femtosecond time scale. This produces a local thermal spike around the ion track through electron-phonon coupling to the atomic structure on the timescale of a few hundred femtoseconds. The localized energy deposition can exceed the bond strength of the semiconductor lattice, even leading to localized melting.[17–39]

At high LET values, the ion tracks are readily visible by transmission electron microscopy. Depending on the atomic number of the ion and its LET, the tracks may be several micrometers long with a diameter of 5–10 nm. An example is shown for GaN irradiated with Pb in Fig. 3,[35] showing both images of the tracks and a histogram of track sizes. GaN ion tracks may contain amorphous material within the track. However, there is a strong tendency for recrystallization. In the case of AlN, it is difficult to detect ion track formation because of an even stronger recrystallization effect.[22,23,35–39] These effects are also seen in molecular dynamics simulations.[30,33] An example is shown in Fig. 4. The physics behind the model is based on excited electrons transferring energy to lattice atoms through electron-phonon coupling. This produces the localized transient lattice heating. At sufficiently high LET, the semiconductor along the ion path melts.[30,31,33] The high temperature in the center of the ion track is subsequently reduced by phonon production or heat conduction by free electrons. Due to athermal defect recombination, the damage production is typically much lower than that given by the simple estimates of the defect concentration given by the nuclear stopping divided by the damage threshold energy.[30,31,33] In the case of ion tracks in GaN, the simulations suggest that N_2 bubbles form within the track. These are shown as dark contrast regions in the tracks of Fig. 4.

For the nuclear stopping mechanism, the incoming ion and the recoiled atoms undergo a series of additional collisions with the lattice atoms. Energy is lost in each of these interactions.[32,36,53–65] At low ion fluences (between 10^{10} and 10^{12} ions/cm^2, depending on ion energy and mass), the damage regions from individual ions do not overlap. The nuclear stopping power is the average energy loss per unit path length. As the incoming ion initially enters the semiconductor, the energy imparted to recoils is high. Therefore, the recoiled atoms can also displace atoms, producing a collision cascade.[63–73] The threshold energy for atom displacement is defined as the smallest kinetic energy required to displace an atom from its substitutional lattice site.[74–94] If the semiconductor crystal

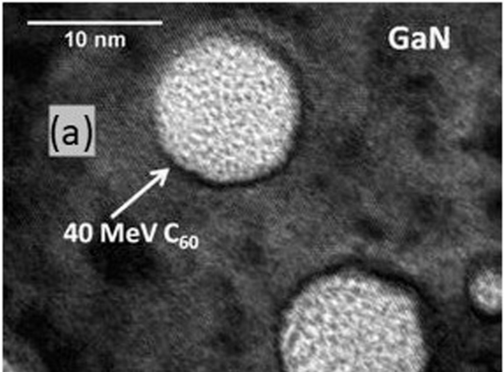

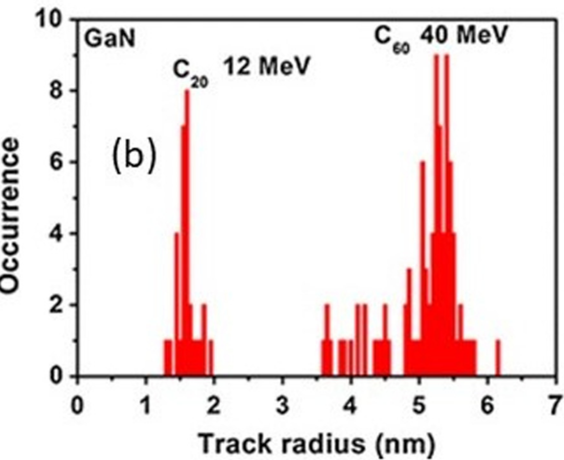

FIG. 3. (a) High resolution plan view: TEM of GaN irradiated with 40 MeV C_{60} (S_e = 59 keV nm^{-1}, 10^{11} ions cm^{-2}). (b) Histogram of track sizes in GaN simultaneously irradiated with 40 MeV C_{60} (S_e = 59 keV nm^{-1}) and 12 MeV C_{20} (S_e = 19 keV nm^{-1}). Reprinted with permission from Sall *et al.*, J. Mater. Sci. **50**, 5214 (2015). Copyright 2010 Springer.

has anisotropic symmetry, the displacement thresholds will also be anisotropic.[53–62] In GaN, there is a large difference between the masses of the elements; therefore, an asymmetry in the damage between Ga and N occurs. Experimentally, the average threshold is 41 eV for the Ga sublattice.[36,37,75] Molecular dynamics simulations gave average thresholds of 45 and 110 eV for Ga and N, respectively,[36,38] while other estimates gave predicted displacement energies of 109 eV for N and 34 eV for Ga. It is difficult to measure these thresholds, and there is significant scatter in the reported data. The thresholds for Si are $T_d = 12.9$ eV and $T_d = 21$ eV.[32,33] Horita *et al.*[58] reported an experimental value for N displacement in GaN as 21.8 eV. These experiments were carried out as irradiation energies were selected to displace only nitrogen atoms. There were two electron traps detected, labeled EE1 (0.13 eV) and EE2 (0.98 eV). These were assigned to nitrogen vacancies V_N (+/0) and nitrogen interstitials N_I (0/−), respectively.[95]

Damage is more significant at low temperatures due to reduced mobility of point defects. At elevated temperatures,

07 April 2024 10:54:22

Published under an exclusive license by the AVS

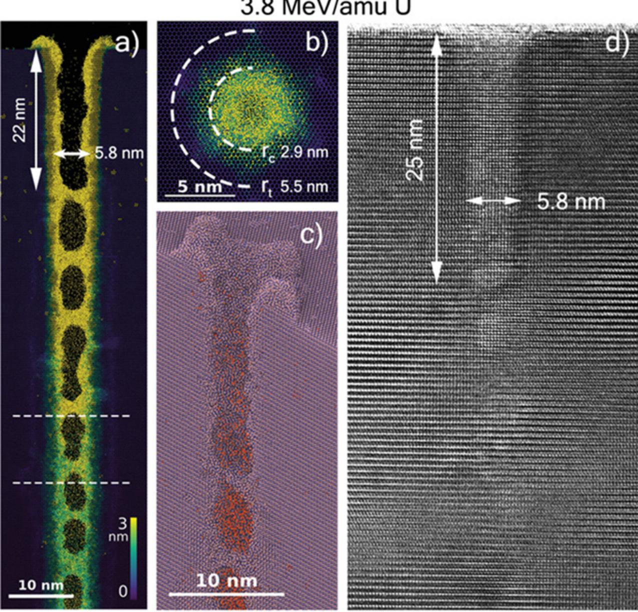

FIG. 4. Simulated (a) cross-sectional, (b) plan-view images, and (c) 3D of a track produced by a 3.8 MeV amu^{-1} U ion (ε_e = 55.15 keV nm^{-1}). The orange balls in (c) represent N_2 molecules. (d) Experimental TEM cross-sectional image of a track produced by the same U ion. The dashed lines in (a) indicate the region from which the image in (b) was taken. The texture within the track is due to nitrogen molecule formation. The simulated and experimental track morphologies are in excellent agreement. Reprinted with permission from Sequeira *et al.*, Small **18**, 2270265 (2022). Copyright 2022 Author(s), licensed under a Creative Commons License.

however, the dynamic annealing of point defects may actually prevent amorphization of the lattice in semiconductors.[32,54] The critical temperature for such prevention of amorphization is a few hundred degrees.

As they lose energy to both nuclear and electronic stopping processes, the incoming ions are eventually slow to thermal velocities (<1 eV). The two stopping processes are almost completely independent of each other. There is also dependence of damage accumulation on the chemical nature of the incoming ions. GaN shows complete amorphization for preimplantation with fluorine, in sharp contrast to preimplantation with neon, phosphorus, or argon, which reduce damage.[37]

Depending on the device bias voltage, the ion energy, and LET, the passage of an ion can lead to perturbations in internal electric fields within the device that are larger than the critical field for avalanche breakdown.

A final point is that the passage of ionizing radiation can alter the diffusivity of point defects in semiconductors.[96–98] The migration energy for ionized defects is generally lower than for nonionized defects. This can produce ionization-stimulated diffusion of point defects and impurities. The Bourgoin mechanism is the athermal recombination of point defects.[98] This obviously reduces effective defect production. This mechanism has been observed for SiC.[21,23,25]

IV. GaN HEMTs AND VERTICAL RECTIFIERS

As pointed out previously, since most GaN-based devices use metal-gates, they do not suffer from oxide damage effects and are tolerant to total ionizing radiation dose effects.[99,100] Figure 5 shows the projected range of high energy protons in GaN (top) and energy loss vs depth for 20 MeV protons, dose 10^{14} cm^{-2} and 1 GeV, and dose 4×10^{13} cm^{-2} protons in GaN (bottom). Note that at 20 MeV, the range is $\sim 10^3$ μm, larger than the thickness of the HEMT structure.

Proton damage for ions >2 MeV energy is only apparent for doses >10^{14} cm^{-2}. This is equivalent to hundreds of years in a low earth orbit. Significant annealing of damage occurs after 500 °C annealing.[101,102] Similar results are reported for alpha particles, while electrons were less damaging than either of these other ions.

For gamma ray irradiation of GaN HEMTs, postirradiation annealing at 200 °C caused some restoration of parameters, such as

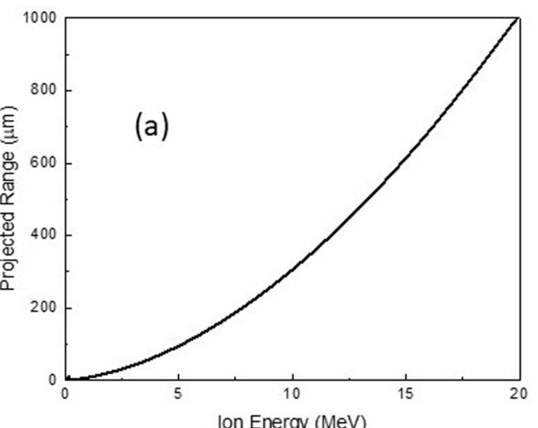

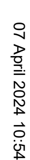

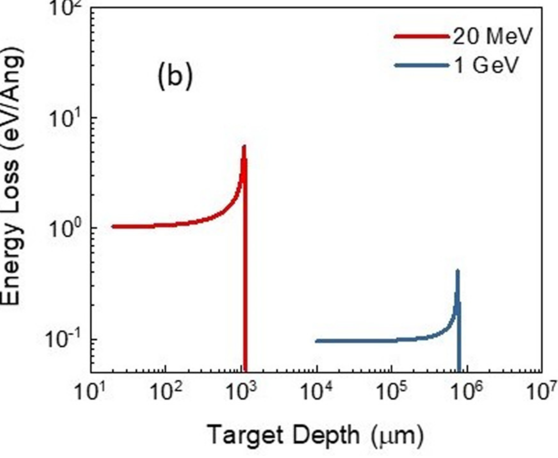

FIG. 5. (a) Range of high energy protons in GaN and (b) energy loss vs depth for 20 MeV protons, dose 10^{14} cm^{-2} and 1 GeV, dose 4×10^{13} cm^{-2} protons in GaN.

Published under an exclusive license by the AVS

diffusion length, drain current, and transconductance.[103–116] A comparison of the carrier removal rates for different types of radiation in GaN, as a function of energy in Fig. 6, shows that protons are the most damaging ones, followed by neutrons, electrons, and gamma rays.[2] Heavy-ion irradiation with >1 GeV Bi or Xe ions at doses $>10^{11}$ cm^{-2} caused large reductions in device source-drain current.[117–121]

Figure 7 shows the deterioration of dc performance of GaN HEMTs after 10 MeV proton damage at a fluence of 10^{14} cm^{-2}. The drain I-V characteristics (a) and transfer characteristics (b) from the HEMTs show reduced current by 20%–50%.[119–131] For 10 MeV irradiated HEMTs, saturation drain current at $V_G = 0$ V was reduced by 24%. Figure 7(b) shows transfer characteristics after irradiation. The extrinsic transconductance, gm, was reduced by 22%, and the threshold voltage showed a positive shift of 0.34 V. The ion bombardment reduces carrier density and electron mobility.[2,119–132] Larger degradation of the gm and a larger Vth shift were obtained for lower proton energies. This corresponds to a higher level of NIEL in the 2D electron gas. SRIM data indicate most of the nuclear stopping damage occurs well into the substrate, at depths of 105, 335, or 672 μm for 5, 10, or 15 MeV, respectively. The two-dimensional electron gas channel (2DEG) of the HEMT is 22 nm below the surface, where the vacancy densities are several orders lower than at the damage peak. For the higher proton energies, there are lower amounts of displacement damage around the 2DEG. Therefore, 5 MeV protons should degrade the HEMT more severely as compared with 10 or 15 MeV protons.

Worsening of GaN HEMT performance occurs at DD levels greater than encountered in most space applications. As shown in Fig. 8,[108] there is a 10× improved performance of GaN compared to GaAs HEMTs in terms of resistance to degradation by irradiation. The susceptibility to displacement damage is larger when devices are biased during irradiation or have had prior hot-carrier stress.[133,134] There are fewer studies of GaN HEMT TID effects, which appear to be a strong function of gate design. In depletion mode Schottky gate devices, Aktas *et al.*[65] reported a 0.1 V threshold shift after 6 Mrad (Si) γ irradiation. For an enhancement mode, p-GaN gate HEMTs, there was no significant shift after 15 Mrad (Si) proton irradiation.[132,133] For 500 krad (Si) γ irradiation, there was a <18% Vth shift.[109]

For irradiation with heavier ions, it is important to calculate the NIEL and ionization loss in the 2DEG region. An example of a typical power HEMT structure is shown in Fig. 9. Since the 2DEG is so close to the surface, heavy ions can create significant damage, as well as create secondary recoil ions that also damage the channel of the HEMT. SRIM simulations of the ionization loss by primary ions and their recoils are shown in Fig. 10(a), while the vacancy concentrations created by the NIEL of the ions and recoils are shown in Fig. 10(b). The SRIM program calculates the ion penetration as a series of independent binary collisions.

Additional temperature-dependent transport measurements of minority carrier lifetime and diffusion length have been reported. Typically, these require the samples to wire-bonded for electron beam-induced current (EBIC) to measure minority carrier

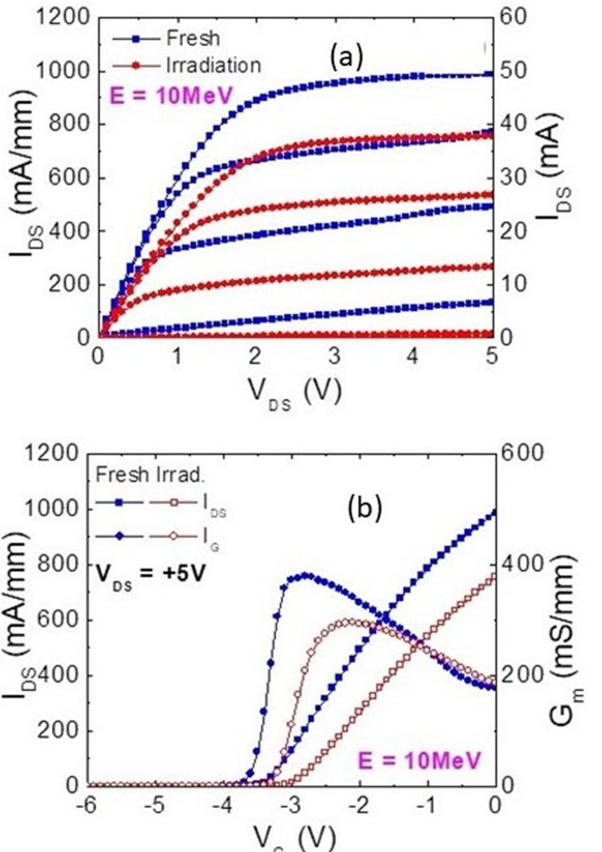

FIG. 7. Drain I-V characteristics (a) and transfer characteristics (b) from GaN HEMTs before and after 10 MeV proton irradiation. Reprinted with permission from Liu *et al.*, J. Vac. Sci. Technol. B **31**, 042202 (2013). Copyright 2013 American Vacuum Society.

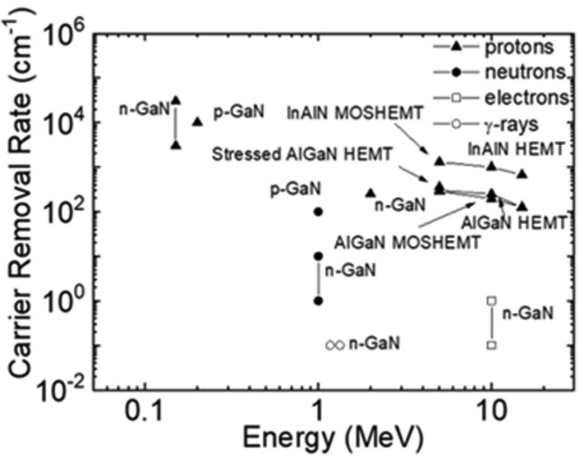

FIG. 6. Compilation of carrier removal rates in GaN-based materials and devices as a function of radiation type and energy.

07 April 2024 10:54:22

Published under an exclusive license by the AVS

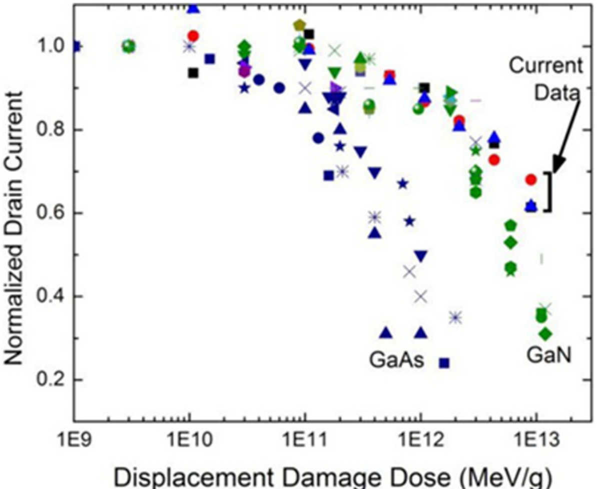

FIG. 8. Degradation of normalized drain current of GaN HEMTs compared to their GaAs counterparts. Reproduced with permission from Weaver *et al.*, ECS J. Solid State Sci. Technol. **5**, Q208 (2016). Copyright 2016 Author(s), licensed under a Creative Commons License.

transport properties, as shown in Figs. 11(a) and 11(b). Lee *et al.*[115] reported dose-dependent effects in AlGaN/GaN HEMTs exposed to 60Co gamma radiation. For doses below ~250 Gy, the minority carrier diffusion length in the HEMTs increased 40%. Similarly, there was an increase in transconductance and reduced gate leakage current after low doses. For doses above ~300 Gy, the performance of HEMTs deteriorated due to the onset of increased carrier scattering from radiation-induced defects.

Figure 12 shows a schematic of the two main degradation mechanisms induced in GaN HEMTs by radiation.[2] The first is creation of midgap trap states, which reduces 2DEG density and drain current. These states are typically charged, which reduces the electron mobility by carrier scattering.

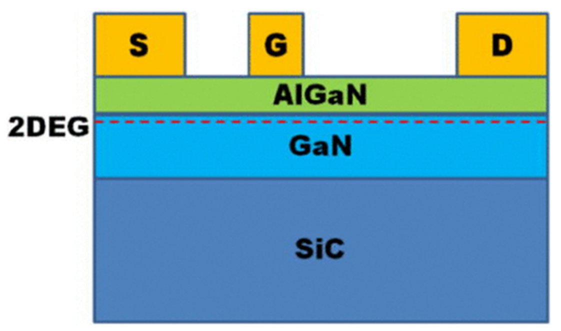

FIG. 9. Schematic of typical high-power GaN HEMT. These are typically grown on SiC substrates to improve the thermal characteristics. A typical thickness of the AlGaN donor layer is 25 nm and the GaN buffer is 3–5 μm.

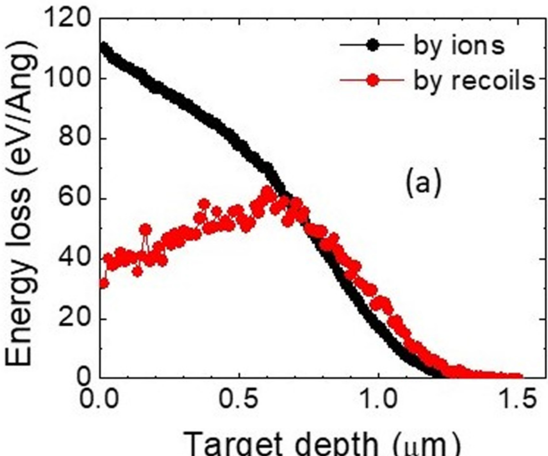

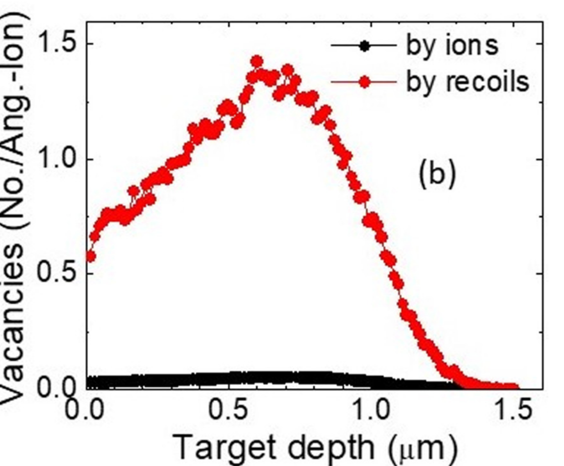

FIG. 10. SRIM simulations of ionization energy loss (a) created by 2 MeV Ge^+ ions and the recoils they created in a power GaN HEMT structure. The ion projected range is ~0.8 μm. The number of vacancies created by the NIEL of the primary ions and the recoils created are shown in (b).

For GaN quasivertical p–i–n rectifiers, irradiation with 150 keV protons reduced both carrier concentration and mobility of p-GaN and n-GaN [1305]. At a proton fluence of 10^{15} p/cm^2, the p-GaN became highly resistive n-GaN. The p-GaN Ohmic contact converted to rectifying behavior, and the main reverse leakage mechanism switched from space-charge-limited current conduction to Ohmic conduction.[134]

Aoshima *et al.*[95] reported a correlation between NIEL and production rates of electron traps at E_C of (0.12–0.20) eV for irradiation of GaN. As shown in Fig. 13, the correlation indicates that the trap states are generated by atomic displacements.

Rasel *et al.*[103–106] recently reported in gamma-irradiated HEMTs that localized regions under tensile stress exhibited higher radiation-induced strain. Co-60 γ-rays have a large mean free path in GaN, as shown in Fig. 14. The gamma rays create damage

07 April 2024 10:54:22

Published under an exclusive license by the AVS

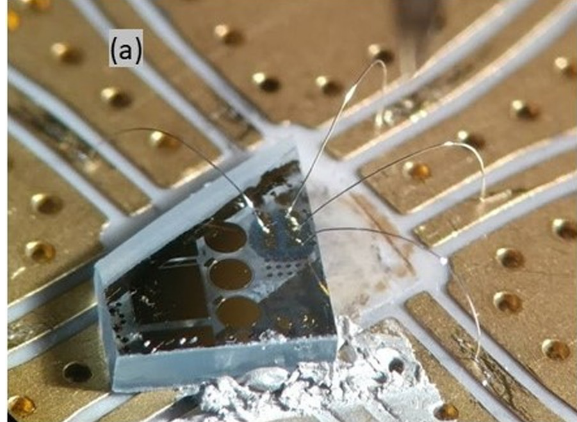

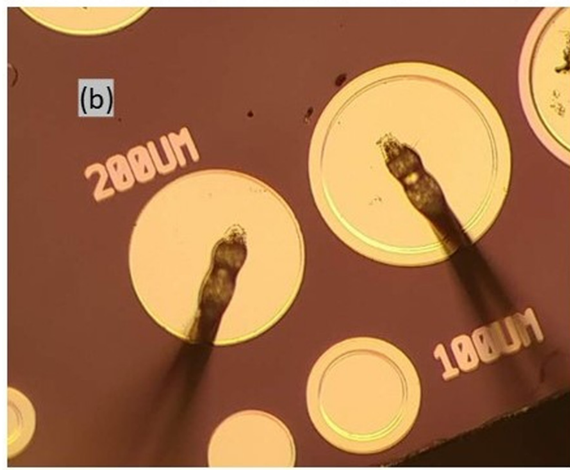

FIG. 11. Optical images (a) and SEM images (b) of wire-bonded GaN HEMTs for transport measurements.

throughout the entire HEMT structure. The suggested mechanism for their observations was dependence of the carrier concentration and mobility in the 2DEG on the tensile stress in the device. When HEMTs were electrically prestressed prior to irradiation, they exhibited a larger threshold voltage shift and a 100× increase in leakage current. In addition, with saturation, current was lowered after irradiation, as shown in Fig. 15. The high electric fields during stressing change the strain in the system and can lead to creation of defects. This was supported by locally relieving strain by creating microtrenches underneath the channel. These reduce the strain within the device, which reduces 2DEG density and mobility. This strain relaxation also reduced the radiation damage created by 10 Mrads (SiO_2) of ^{60}Co-gamma exposure.

Rasel *et al.*[103,104] also demonstrated a novel nonthermal annealing process for gamma-induced damage in GaN HEMTs using the electron momentum from short, high current density pulses to anneal defects. This process was used on 5 Mrad dose (SiO_2) irradiated HEMTs and restored saturation current and maximum transconductance, while the threshold voltage was

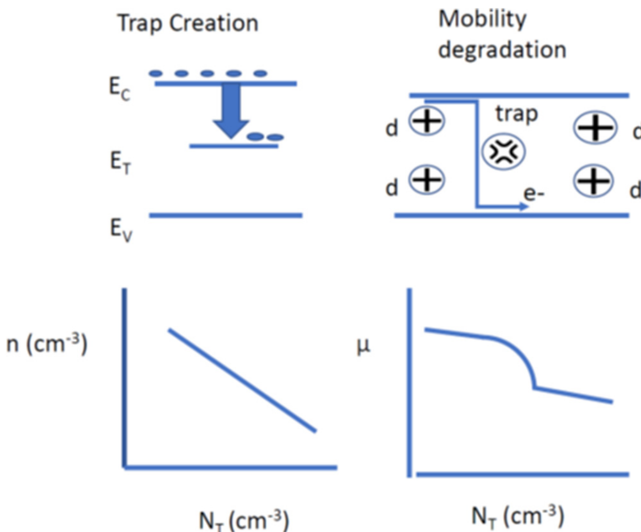

FIG. 12. Schematic of main degradation mechanisms in GaN HEMTs exposed to radiation. The displacement damage created midgap states that trap carriers and reduce carrier mobility.

partially recovered. By sharp contrast, conventional thermal annealing at 300 °C degraded the irradiated device characteristics.

The susceptibility for SEE in GaN HEMTs increases with voltage.[107] SEB in ∼600 V p-gate parts occurs at ∼50% of rating at

07 April 2024 10:54:22

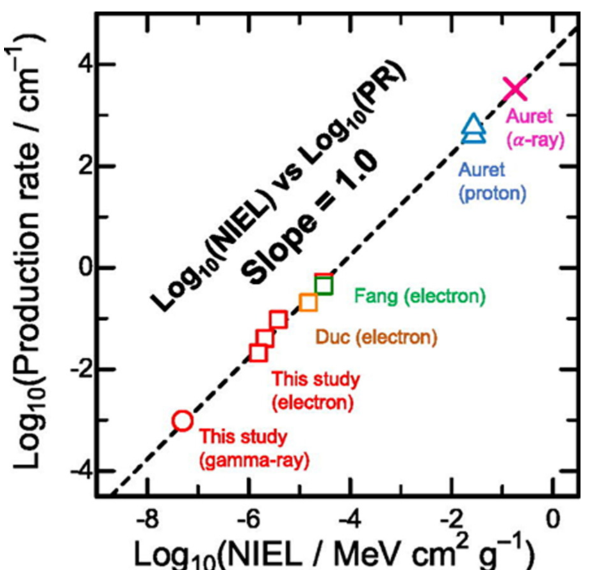

FIG. 13. Production rates of electron traps at E_C of (0.12–0.20) eV as a function of NIEL for electrons, protons, α-rays, and gamma rays. Reprinted with permission from Aoshima *et al.*, Appl. Phys. Lett. **122**, 012106 (2023). Copyright 2023 American Institute of Physics.

Published under an exclusive license by the AVS

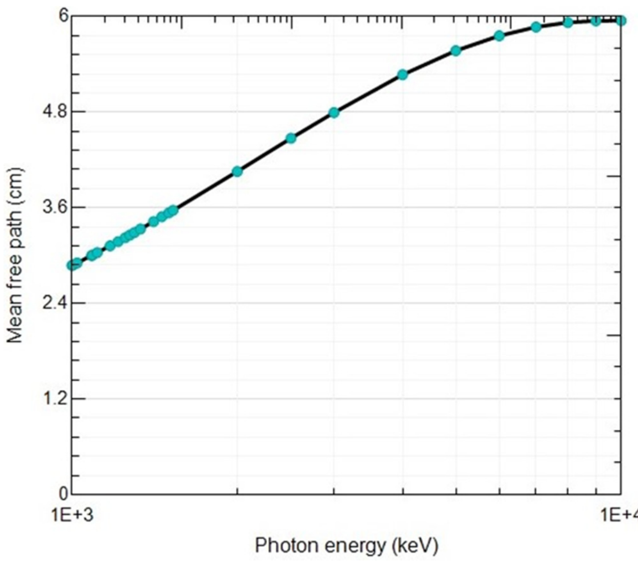

FIG. 14. Mean free path of gamma rays in GaN as a function of energy. The plot was calculated from the code in Hila *et al.*, Rad. Phys. Chem. **182**, 109331 (2021). Copyright 2021 Elsevier.

LET ∼40 MeV cm^2/mg (Si). The burnout occurs at insulators for source or gate field plates. GaN HEMTs have several catastrophic SEE failure modes. Figure 16 shows single-event burnout in Xe irradiated HEMTs at 380 V bias [1038]. The first failure mode was creation of a leakage path from drain to an Si substrate through the

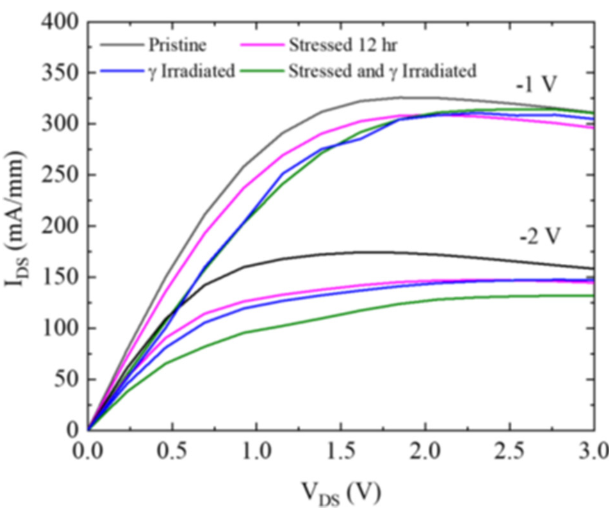

FIG. 15. Effect of gamma irradiation on the forward I-V curve for zero gate voltage at different device conditions. Reprinted with permission from Rasel *et al.*, Appl. Phys. Lett. **120**, 124101 (2022). Copyright 2022 American Institute of Physics.

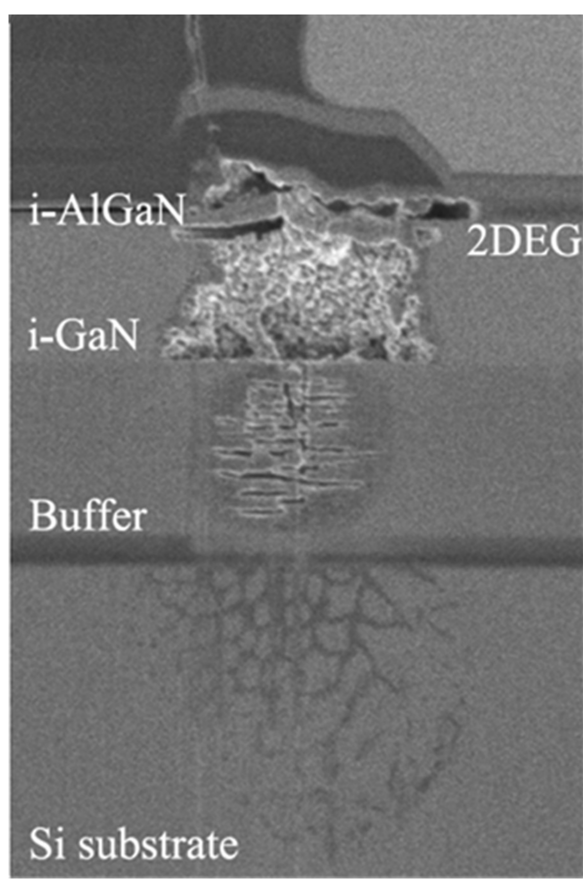

FIG. 16. Heavy-ion-induced single-event burnout in GaN/AlGaN HEMT. The device was damaged during Xe ion irradiation at V_{DS} = 380 V. Reprinted with permission from Mizuta *et al.*, IEEE T. Nucl. Sci. **65**, 1956 (2018). Copyright 2018 IEEE.

buffer layer. The other mode was damage between the drain and source. In these experiments, the damage was produced by ions with LET ≥30.6 MeV/(mg/cm^2) at normal incidence.

V. GaN PHOTONIC DEVICES

GaN-based light-emitting diodes (LEDs) and laser diodes are commercialized for the UV-visible range, using GaN/InGaN for the green/blue region of the spectrum and GaN/AlGaN heterostructures for the UV. These devices operate in forward bias, to drive electrons and holes from either side of a p-n junction together to recombine and emit photons whose wavelength is determined by the bandgap of the active region. Radiation-induced defects act as both carrier trap states and recombination centers, enhancing nonradiative recombination and reducing carrier concentration.[134–141] The domination of such processes over radiative spontaneous and stimulated emission degrades LED or laser performance. Osiński *et al.*[142] reported improved radiation hardness of nitride-based LEDs relative to GaAs LEDs. The output

07 April 2024 10:54:22

Published under an exclusive license by the AVS

power of AlGaN/InGaN/GaN green LEDs after 2 MeV protons at 10^{12} cm^{-2} decreased 40%. Gaudreau *et al.*[143] reported 2 MeV protons at $>3\times10^{12}$ cm^{-2} reduced both electrical and optical performance of AlGaN/InGaN/AlGaN blue LEDs, with light output reduced by more than 99% for 10^{15} cm^{-2} proton fluence. The optical properties were observed to be degraded at a faster rate than that of the electrical properties. This was a result of the higher nonradiative transitions caused by the presence of radiation-induced defect states. Khanna *et al.*[144] reported the proton energy dependence of light output degradation of blue LEDs over the range of 2–115 MeV.

The effects of proton irradiation on InGaN/GaN blue LEDs were reported by Kim *et al.*[78,81,145] and are summarized in Figs. 17(a)–17(c). The LEDs were irradiated with protons at 340 keV and fluences of 5×10^{10}–10^{14} cm^{-2}. Both current–voltage and light output–current characteristics were gradually degraded as increasing proton fluence. The reverse recovery time before and after 10^{14} cm^{-2} proton fluence decreased from 31.0 to 27.6 ns.[78,81,145] Ion tracks in GaN-based devices have not been observed in LED structures, and it will be interesting to see if the absence of a high electric field region still leads to the type of track observed in electronic devices with high reverse biases.[146–150]

There has been less work on radiation damage in GaN-based lasers.[144] In general, it is found that the threshold current increases with radiation fluence, with neutrons being more damaging than γ-rays because of higher effectiveness in producing displacement defects. This increase is caused by nonradiative recombination centers competing with radiative recombination sites. Gamma irradiation does not cause significant degradation at doses lower than 10^{7}–10^{8} rad if the irradiation is performed under lasing conditions. By contrast, neutron irradiation causes significant damage in GaN laser diodes at fluences $>10^{13}$–10^{14} cm^{-2}.

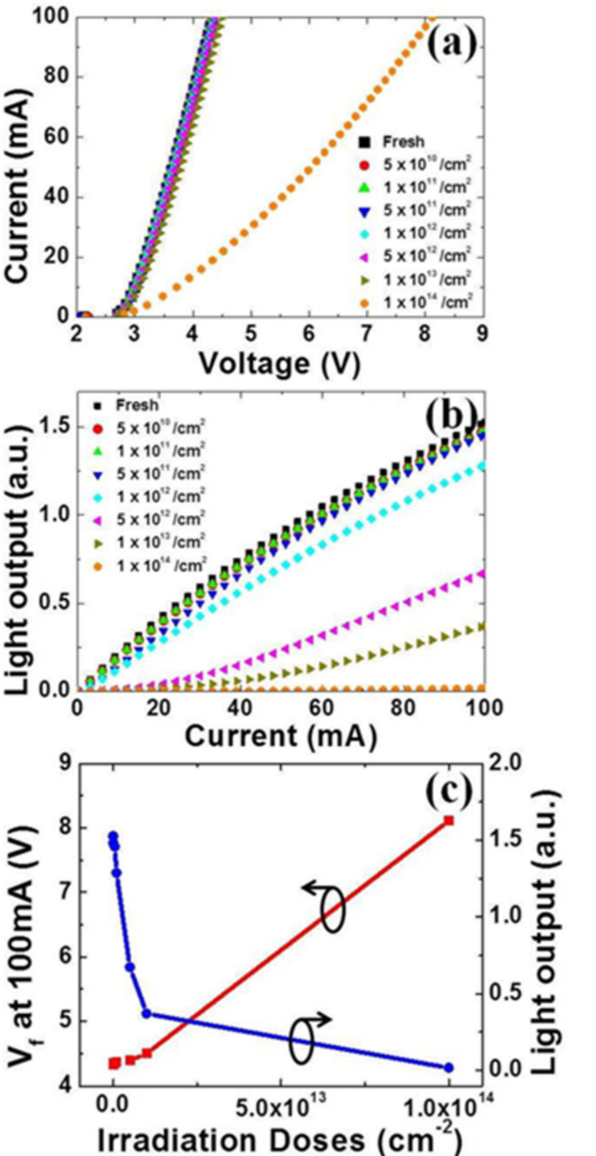

FIG. 17. (a) Current–voltage and (b) the light output–current characteristics of the InGaN/GaN blue LEDs prior to and after 340 keV proton irradiations with various doses, respectively. (c) The change of the forward voltage at an injection current of 100 mA and a light output as a function of irradiation doses. Reprinted with permission from Kim *et al.*, J. Vac. Sci. Technol. B **33**, 051215 (2015). Copyright 2015 American Vacuum Society.

VI. SiC MOSFETs AND BJTs

SiC devices have a tenfold higher breakdown field than Si devices. Thus, the drift layer within an SiC power device can be thinner or have higher doping levels. Commercial 4H-SiC power MOSFETs irradiated with gamma rays become inoperative after 300 kRad.[151–159] A 4H-SiC power bipolar junction transistor (BJT) suffered small gain degradation after a dose of 8.7 MRad. Gamma rays usually produce little change in SiC devices without gate oxides, even up to 100 Mrad. This indicates that TID effects in the gate oxide are the dominant effect in gamma-exposed SiC devices, although SiC MOSFETs can be TID-robust despite their relatively thick oxides. Typically, the currently available devices degrade at >300 krad (Si).

Irradiation with protons, neutrons, and electrons creates displacement damage in SiC devices at high fluences.[151–159] Significant degradation in I-V characteristics of 6H-SiC transistors occurs for neutron fluences $>5\times10^{15}$ cm^{-2}.[154–162]

SiC power MOSFETs are susceptible to heavy-ion irradiation-induced SEB at ground level due to terrestrial neutrons. Figure 18 shows heavy-ion-induced single-event burnout in an SiC diode.[154] Permanent changes in the mechanical properties of SiC can also be induced by ion bombardment.[163]

The response to single-event effects is the biggest issue with SiC power devices and their radiation stability. Some of the different SEEs in SiC Schottky diodes include transient effects due to charge injection, permanently increased leakage current, and catastrophic burnout. These occur at different bias levels, as shown in Fig. 19.[157,164–204] The threshold for ion-induced leakage current

07 April 2024 10:54:22

Published under an exclusive license by the AVS

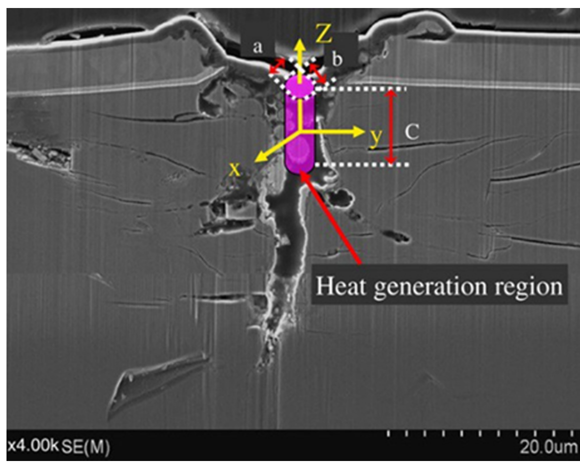

FIG. 18. Heavy-ion-induced single-event burnout in an SiC diode. Reprinted with permission from Shoji *et al.*, Jpn. J. Appl. Phys. **53**, 04EP03 (2014). Copyright 2014 The Japan Society of Applied Physics.

and single-event burnout saturates with linear energy transfer (LET). SEB produces destructive failure and is electric field dependent. For example, 650–3300 V diodes fail at a similar fraction of rated V_R.

Displacement damage to first order does not depend on field and occurs without biasing the device. If just the level of NIEL is considered during single-event strikes, it would be predicted that a much lower amount of leakage current in SiC power devices per ion strike would be induced. The permanent damage occurring during these catastrophic strikes also results from Joule heating along the ion track. TEM observations indicate that the damage

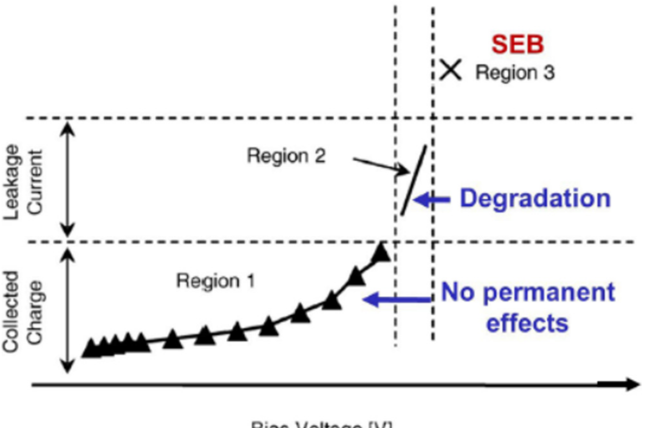

FIG. 19. Characteristic regions observed by heavy-ion irradiations on SiC Schottky diodes. (The image was derived from experimental data with Ar ion.) Reprinted with permission from Kuboyama *et al.*, IEEE T. Nucl. Sci. **66**, 1688 (2019). Copyright 2019 IEEE.

site diameter is approximately the same size as the ion track diameter.[151–153] The passage of these ions creates thermal damage, which has different effects to displacement damage. Experimentally, it is seen that the degradation has little dependence on the rated breakdown voltage. For example, 600–1700V rectifiers all have the same critical power density threshold.[157]

In terms of single-event burnout, the key components for SEB in SiC Schottky diodes have been identified via TCAD simulations. One important factor is the duration of a high E-field at the Schottky contact,[205–213] which impacts the onset of impact ionization and thermal runaway at the contact.[153] SEEs in SiC MOSFETs include latent gate damage, permanent increased leakage current, and formation of drain-gate or drain-source leakage pathways.[208] Drain-gate leakage is the main degradation in junction FETs (JFETs).

Gate damage in MOSFETs is minimized for lower LET or light ions. The mechanism suggested by Abbate *et al.*[204,205] is that the ion strike causes a high field at the interface with the oxide, high hole trapping in oxide, a shift of an SiC electric field across oxide, resulting in fast current injection. There is Poole–Frenkel-like rapid emission of holes from oxide traps and Fowler–Nordheim tunneling of holes across the SiC/SiO_2 interface. The SEB occurs at ∼50% of rated bias. Figure 20(a) shows degradation thresholds as functions of bias and LET, while experimental data are shown in Fig. 20(b). Mitigating these risks is problematic if SEB protection circuitry is too slow to protect against ion-induced transients.

In SiC, heat removal is by acoustic phonons, but these take several ns to start conducting heat away. E-h pairs form along the track of the incoming ion, and then optical phonons are created on a time scale of 1–5 ps. However, acoustic phonons to conduct heat away are not formed until ∼1 ns.[189,197,207] The higher high peak fields in SiC compared to Si means that there is a 2 order of magnitude higher heat generation density. This leads to a rapid rise in the temperature, given by $\Delta T = \text{time} \times \text{power/heat capacity (C)}$, where $C \propto$ heated volume. The expected temperature rises are beyond the melting point, and SiC sublimation occurs in picoseconds.[154,195,197]

To summarize SiC, Schottky diode susceptibility to SEB occurs at <50% of the rated avalanche bias. By sharp contrast, Si Schottky diodes do not fail at this bias level, with half passing at 100%.[157] SEB occurs as a result of the faster recombination of electrons and holes at the high field contact.[157] The resulting lower carrier density increases the electric field at the contact and initiates impact ionization. The higher field is sustained for several hundred ps, inducing Joule heating, which causes thermal runaway. The increased temperature causes more electron injection from the Schottky contact and recombination with holes. The positive feedback produces thermal runaway. Since the peak electric field in SiC power devices is an order of magnitude higher than in Si devices, the heat generation density in SiC devices is 2 orders of magnitude higher since the Joule power density is proportional to electric field squared. TCAD simulations indicate that thicker, lower doped, epitaxial layers increase the threshold for ion-induced SEB.

Terrestrial neutron exposures of commercial SiC devices with planar, trench, and double-trench architecture were found to produce different failure mechanisms.[206]

In the thesis work by Suvanam,[214] studies were performed on radiation effects on MOS structures, 4H-SiC BJT, and 4H-SiC

07 April 2024 10:54:22

Published under an exclusive license by the AVS

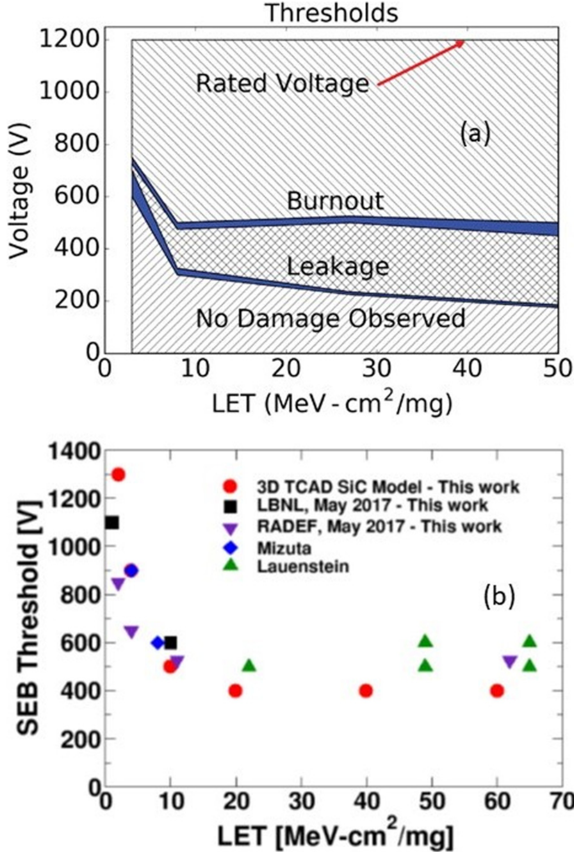

FIG. 20. (a) Measured degradation mode thresholds as functions of applied bias and LET. The width of the line indicates the minimum voltage at which burnout was observed and the maximum voltage with no burnout. (b) SEB threshold voltage for 1.2 kV SiC MOSFETs collected from several heavy-ion experiments. Adapted from J.-M. Lauenstein, "Getting SiC power devices off the ground: Design, testing, and overcoming radiation threats," *Microelectronics Reliability and Qualification Working (MRQW) Meeting*, El Segundo, CA, February 2018; see: https://ntrs.nasa.gov/search.jsp?R=20180006113.

circuits using 50 keV Ar^+, 3 MeV protons, and gamma radiation. Radiation effects depended on the device structure and design and also on the radiation dose. Compared to Si-technology,[68] the 4H-SiC BJTs showed 1 order of magnitude higher radiation tolerances.

The radiation hardness of a 4H-SiC bipolar junction transistor exposed to 332 Mrad gamma radiation and protons showed that they were 100× more tolerant to gamma radiation than Si.[214–217] 4H-SiC devices and circuits irradiated with 3 MeV protons showed 10× higher tolerance compared to Si. For 4H SiC integrated OR-NOR logic circuits, no reduction in logic swing was observed to proton doses of 10^{12} cm^{-2} and gamma doses of 10^8 Mrad. SiC BJTs irradiated with gamma rays showed recovery to 92% of the preradiation condition after annealing at 420 °C for 1800s.[214]

In summary for SiC devices, there are still issues with stability of the SiC/SiO_2 interface in radiation environments. The main cause for degradation due to radiation is ionization effects in the dielectric and interface layers. The radiation stability is still 10×–100× higher than Si.

VII. SUMMARY AND CONCLUSIONS

The three main types of radiation effects,[218–225] TID, DD, and SEE, have different effects on SiC and GaN devices. In MOS devices, TID radiation creates traps in the oxide, which alters the local electric field at the interface with the semiconductor, and this can screen the externally applied voltage, changing the device operating characteristics. TID is due to the ionization created by the radiation as it passes through the semiconductor and dielectric. DD occurs when the incident atom has kinetic energy higher than the displacement threshold energy of the semiconductor. Under these conditions, the incoming ion can displace lattice atoms, producing Frenkel pairs. The device parameters most sensitive to displacement damage are minority carrier lifetime, diffusion length, mobility, and carrier concentration. The production rate of many traps observed in SiC and GaN after irradiation is directly proportional to energy loss per unit length of the incident ions due to displacement processes (NIEL). This shows that they are due to atomic displacements.

SEEs occur when an energetic particle traverses the semiconductor, producing electron-hole pairs along the track. While the e-h pairs recombine, they can produce a transient response in the device. Most of the SEEs disappear within picoseconds after the generated charges diffuse and recombine. While these are not destructive, if there is a high enough LET and strong electric fields are present at the device operating conditions, destructive mechanisms can occur.

Although these three types of damage are independent of each other, they obviously occur simultaneously during a radiation event.[226–228] As an example, a high energy proton will create electron-hole pairs while also displacing lattice atoms in the SiC or GaN lattice atoms. In other words, the same incoming ions induce both TID and DD effects.

All commercially available SiC power devices, including Schottky and pin diodes, MOSFETs, and JFETs, show catastrophic single-event-induced failure at ≲50% of their rated voltages. The very high electric fields in such devices are the cause of failure at high ion LET values. There is also noncatastrophic damage at biases ~10% of rated values.

Photonic devices show changes in the optical output intensity at lower radiation levels than those at which changes in the electrical parameters are noted. There has been little examination of using forward-bias injection of carriers to try to induce athermal annealing of radiation damage in GaN-based LEDs and lasers.

Overall, while SiC and GaN electronic devices are more robust against degradation by TID and DD effects during radiation exposure than Si devices, the current designs show higher sensitivity to SEE, especially catastrophic burnout. Optimized design of active layer thicknesses and doping should partially mitigate these effects.

We can summarize the main conclusions as follows:

(1) GaN and SiC devices are more resistant to total dose radiation damage than Si or GaAs due to their higher bond strengths and higher defect recombination rates.[2,15]

07 April 2024 10:54:22

Published under an exclusive license by the AVS

(2) The wide bandgap devices are more susceptible to single-event related failures due to the high electric fields present, which leads to thermal and electrical runaway. The only method to mitigate this involves operating them at lower than their rated voltages.[2,162,193]
(3) TID effects are usually only present in devices with MOS gates, and thus, this is significant in SiC MOSFETs.[157,179,180] GaN devices still mainly employ metal-gates and are relatively immune to ID effects.
(4) Optimized design of devices that are specifically designed for improved radiation hardness will require significant investments in modeling and simulation.[204,210]

ACKNOWLEDGMENTS

This work was performed as part of the Interaction of Ionizing Radiation with Matter University Research Alliance (IIRM-URA), sponsored by the Department of the Defense, Defense Threat Reduction Agency under Award No. HDTRA1-20-2-0002. The content of the information does not necessarily reflect the position or the policy of the federal government, and no official endorsement should be inferred. A.H. also acknowledges support from the U.S. National Science Foundation (ECCS No. 2015795). The work at UF was also supported by the NSF DMR 1856662.

AUTHOR DECLARATIONS

Conflict of Interest

The authors have no conflicts to disclose.

Author Contributions

S. J. Pearton: Conceptualization (equal); Data curation (equal); Formal analysis (equal); Funding acquisition (equal); Writing – original draft (equal). **Xinyi Xia:** Conceptualization (equal); Data curation (equal); Formal analysis (equal); Investigation (equal); Methodology (equal); Writing – original draft (equal). **Fan Ren:** Conceptualization (equal); Data curation (equal); Formal analysis (equal); Funding acquisition (equal); Investigation (equal); Methodology (equal); Project administration (equal); Writing – original draft (equal). **Md Abu Jafar Rasel:** Conceptualization (equal); Data curation (equal); Formal analysis (equal); Funding acquisition (equal); Investigation (equal); Methodology (equal); Visualization (equal). **Sergei Stepanoff:** Conceptualization (equal); Data curation (equal); Formal analysis (equal); Investigation (equal); Methodology (equal); Writing – original draft (equal). **Nahid Al-Mamun:** Conceptualization (equal); Data curation (equal); Formal analysis (equal); Investigation (equal); Methodology (equal); Writing – original draft (equal). **Aman Haque:** Conceptualization (equal); Data curation (equal); Formal analysis (equal); Investigation (equal); Methodology (equal); Project administration (equal); Writing – original draft (equal). **Douglas E. Wolfe:** Conceptualization (equal); Data curation (equal); Formal analysis (equal); Investigation (equal); Methodology (equal); Writing – original draft (equal).

DATA AVAILABILITY

Data sharing is not applicable to this article as no new data were created or analyzed in this study.

REFERENCES

[1]R. J. Kaplar, J. Neely, D. Huber, and L. Rashkin, IEEE Power Electron. Mag. **4**, 36 (2017).
[2]S. J. Pearton *et al.*, ECS J. Solid State Sci. Technol. **10**, 055008 (2021).
[3]M. Tadjer, J. Lyons, J. Nepal, J. Freitas, A. Koehler, and G. Foster, ECS J. Solid State Sci. Technol. **8**, Q3187 (2019).
[4]G. L. Harris, *Properties of Silicon Carbide* (IEE INSPEC, London, 1995).
[5]Y. Goldberg, M. E. Levinshtein, and S. L. Rumyantsev, in *Properties of Advanced Semiconductor Materials*, edited by M. E. Levinshtein, S. L. Rumyantsev, and M. S. Shur (John Wiley, New York, 2001).
[6]M. Bass, G. Li, and E. Van Stryland, *Handbook of Optics*, 3rd ed. (Optical Society of America, New York, 2010), Vol. IV.
[7]J. F. Shakelfold and W. Alexander, *CRC Materials Science and Engineering Handbook*, 3rd ed. (CRC, Boca Raton, FL, 2000).
[8]J. Holmes, A. M. Francis, I. Getreu, M. Barlow, A. Abbasi, and H. A. Mantooth, J. Microelectron. Electron. Packag. **13**, 143 (2016).
[9]C. Wilson, C.-M. Zetterling, and W. T. Pike, "Venus long-life surface package (VL2SP)," (2016); see https://arxiv.org/abs/1611.03365.
[10]A. Rahman *et al.*, IEEE J. Emerg. Sel. Top. Power Electron. **4**, 935 (2016).
[11]P. G. Neudeck, L. Chen, R. D. Meredith, D. Lukco, D. J. Spry, L. M. Nakley, and G. W. Hunter, IEEE J. Electron Devices Soc. **7**, 100 (2019).
[12]W. F. Koehl, B. B. Buckley, F. J. Heremans, G. Calusine, and D. D. Awschalom, Nature **479**, 84 (2011).
[13]S. J. Pearton, F. Ren, E. Patrick, M. E. Law, and A. Y. Polyakov, ECS J. Solid State Sci. Technol. **5**, Q35 (2016).
[14]Daniel M. Fleetwood, En Xia Zhan, Ronald D. Schrimpf, and Sokrates T. Pantelides, IEEE Trans. Nucl. Sci. **69**, 1105 (2022).
[15]B. C. Letson, S. Barke, P. Wass, G. Mueller, F. Ren, S. J. Pearton, and J. W. Conklin, J. Vac. Sci. Technol. A **41**, 013202 (2023).
[16]S. J. Pearton, Aman Haque, Ani Khachatrian, Adrian Ildefonso, Leonid Chernyak, and Fan Ren, ECS J. Solid State Sci. Technol. **10**, 075004 (2021).
[17]S. S. Suvanam, S.-I. Kuroki, L. Lanni, R. Hadayati, T. Ohshima, T. Makino, A. Hallén, and C. M. Zetterling, IEEE Trans. Nucl. Sci. **64**, 852 (2017).
[18]C.-M. Zetterling *et al.*, Semicond. Sci. Technol. **32**, 034002 (2017).
[19]M. Ekström, B. G. Malm, and C.-M. Zetterling, IEEE Electron Device Lett. **40**, 670 (2019).
[20]A. Mantooth, C.-M. Zetterling, and A. Rusu, IEEE Spectr. **58**, 24 (2021).
[21]M. Asiatici, A. C. Fischer, H. Rödjegård, S. Haasl, G. Stemme, and F. Niklaus, Sens. Actuators, A **238**, 361 (2016).
[22]K. Nordlund *et al.*, Nat. Commun. **9**, 1084 (2018).
[23]Kai Nordlund *et al.*, J. Nucl. Mater. **512**, 450 (2018).
[24]J. Nord, K. Nordlund, and J. Keinonen, Phys. Rev. B **68**, 184104 (2003).
[25]Yanwen Zhang and William J. Weber, Appl. Phys. Rev. **7**, 041307 (2020).
[26]W. J. Weber, D. M. Duffy, L. Thomé, and Y. Zhang, Curr. Opin. Solid State Mater. Sci. **19**, 1 (2015).
[27]Y. Zhang *et al.*, Curr. Opin. Solid State Mater. Sci. **21**, 285 (2017).
[28]W. J. Weber and Y. Zhang, Curr. Opin. Solid State Mater. Sci. **23**, 100757 (2019).
[29]S. Agarwal, Q. Chen, T. Koyanagi, Y. Zhao, S. J. Zinkle, and W. J. Weber, J. Nucl. Mater. **526**, 151778 (2019).
[30]Lauren Nuckols, Miguel L. Crespillo, Chen Xu, Eva Zarkadoula, Yanwen Zhang, and William J. Weber, Acta Mater. **199**, 96 (2020).
[31]K. Nordlund, M. Ghaly, R. S. Averback, M. Caturla, T. Diaz de la Rubia, and J. Tarus, Phys. Rev. B **57**, 7556 (1998).
[32]J. W. Corbett and G. D. Watkins, Phys. Rev. **138**, A555 (1965).
[33]J. J. Loferski and P. Rappaport, J. Appl. Phys. **30**, 1296 (1959).

07 April 2024 10:54:22

Published under an exclusive license by the AVS

[34]R. E. Stoller, M. B. Toloczko, G. S. Was, A. G. Certain, S. Dwaraknath, and F. A. Garner, Nucl. Instrum. Methods Phys. Res., Sect. B **310**, 75 (2013).
[35]M. C. Sequeira, F. Djurabekova, K. Nordlund, J. G. Mattei, I. Monnet, C. Grygiel, E. Alves, and K. Lorenz, Small **18**, 2270265 (2022).
[36]M. Sall, I. Monnet, F. Moisy, C. Grygiel, S. Jublot-Leclerc, S. Della–Negra, M. Toulemonde, and E. Balanzat, J. Mater. Sci. **50**, 5214 (2015).
[37]S. O. Kucheyev, H. Timmers, J. Zou, J. S. Williams, C. Jagadish, and G. Li, J. Appl. Phys. **95**, 5360 (2004).
[38]J. Nord, J. K. Nordlund, J. Keinonen, and K. Albe, Nucl. Instrum. Methods Phys. Res., Sect. B **202**, 93 (2003).
[39]K. Nordlund, Comput. Mater. Sci. **3**, 448 (1995).
[40]S. A. Vitusevich *et al.*, Phys. Status Solidi A **195**,101 (2003).
[41]E. A. Wendler, E. Kamarou, K. Alves, K. Gärtner, and W. Wesch, Nucl. Instrum. Methods Phys. Res., Sect. B **206**, 1028 (2003).
[42]E. A. Wendler, W. Wesch, E. Alves, and A. Kamarou, Nucl. Instrum. Methods Phys. Res., Sect. B **218**, 36 (2004).
[43]W. K. Tobiska *et al.*, Space Weather **14**, 1053 (2016).
[44]P. P. Beck, P. Ambrosi, U. Schrewe, and K. O'Brien, ACREM (Aircrew Radiation Exposure Monitoring), Final report of European Commission Contract No. F14P-CT960047, OEFZS, Rep. G-0008, 1999.
[45]P. Beck, M. Latocha, S. Rollet, and G. Stehno, Adv. Space Res. **36**, 1627 (2005).
[46]P. Beck, C. Dyer, N. Fuller, A. Hands, M. Latocha, S. Rollet, and F. Spurny, Radiat. Prot. Dosim. **136**, 297 (2009).
[47]O. Burda, T. Sato, and F. Wissmann, J. Radiol. Prot. **33**, 339 (2013).
[48]P. Cannon, *Extreme Space Weather: Impacts on Engineered Systems and Infrastructure* (Royal Academy of Engineering, London, 2013).
[49]C. Dyer *et al.*, IEEE Trans. Nucl. Sci. **56**, 3415 (2009).
[50]C. S. Dyer, A. J. Sims, J. Farren, and J. Stephen, IEEE Trans. Nucl. Sci. **37**, 1929 (1990).
[51]E. B. Yakimov *et al.*, Appl. Phys. Lett. **118**, 202106 (2021).
[52]M. V. S. Chandrashekhar, C. I. Thomas, and M. G. Spencer, Appl. Phys. Lett. **89**, 042113 (2006).
[53]A. A. Lebedev, A. M. Ivanov, and N. B. Strokan, Semiconductors **38**, 125 (2004).
[54]C. A. Klein, J. Appl. Phys. **39**, 2029 (1968).
[55]T. Kobayashi, Appl. Phys. Lett. **21**, 150 (1972).
[56]R. C. Alig and S. Bloom, Phys. Rev. Lett. **35**, 1522 (1975).
[57]S. Butera, G. Lioliou, A. B. Krysa, and A. M. Barnett, Nucl. Instrum. Methods Phys. Res., Sect. A **879**, 64 (2018).
[58]Masahiro Horita, Tetsuo Narita, Tetsu Kachi, and Jun Suda, Appl. Phys. Lett. **118**, 012106 (2021).
[59]J. S. Williams, Mater. Sci. Eng. A **253**, 8 (1998).
[60]J. W. Steeds, Nucl. Instrum. Methods Phys. Res., Sect. B **269**, 1702 (2011).
[61]G. A. Umana-Membreno, J. M. Dell, T. P. Hessler, B. D. Nener, G. Parish, L. Faraone, and U. K. Mishra, Appl. Phys. Lett. **80**, 4354 (2002).
[62]V. V. Emtsev *et al.*, Semicond. Sci. Technol. **15**, 73 (2000).
[63]Chandan Sharma, Rajendra Singh, Der-Sheng Chao, and Tian-Li Wu, Semicond. Sci. Technol. **34**, 065024 (2019).
[64]Gu Wenping, Chen Chi, Duan Huantao, Hao Yue *et al.*, J. Semiconductors **30**, 044002 (2009).
[65]O. Aktas, A. Kulieva, V. Kumara, R. Schwindt, S. Toshkov, D. Costescu, J. Stubbin, and I. Adesida, Solid-State Electron. **48**, 471 (2004).
[66]C. Schwarz *et al.*, Appl. Phys. Lett. **102**, 062102 (2013).
[67]In Hwan Lee *et al.*, Appl. Phys. Lett. **110**, 112102 (2017).
[68]Shihyun Ahn, ByungJae Kim, Yi Hsuan Lin, Fan Ren, S. J. Pearton, Gwangseok Yang, Jihyun Kim, and Ivan Kravchenko, J. Vac. Sci. Technol. B **34**, 051202 (2016).
[69]B. J. Kim, S. Ahn, Fan Ren, S. J. Pearton, G. Yang, and J. Kim, J. Vac. Sci. Technol. B **34**, 041231 (2016).
[70]Ya Shi Hwang *et al.*, J. Vac. Sci. Technol. B **31**, 022206 (2013).
[71]L. Liu, C. V. Cuervo, Y. Xi, F. Ren, S. J. Pearton, H. Y. Kim, J. Kim, and I. I. Kravchenko, J. Vac. Sci. Technol. B **31**, 042202 (2013).
[72]A. Y. Polyakov, S. J. Pearton, P. Frenzer, F. Ren, L. Liu, and J. Kim, J. Mater. Chem. C **1**, 877 (2013).
[73]M. P. King *et al.*, IEEE Trans. Nucl. Sci. **62**, 2912 (2015).
[74]L. Lv *et al.*, IEEE Trans. Nucl. Sci. **64**, 643 (2017).
[75]K. H. Chow, G. D. Watkins, A. Usui, and M. Mizuta, Phys. Rev. Lett. **85**, 2761 (2000).
[76]Yun Tang, Lei Wang, Xiaowu Cai, Peng Lu, and Bo Li, Appl. Phys. Lett. **122**, 022101 (2023).
[77]S. J. Pearton, R. Deist, F. Ren, L. Liu, A. Y. Polyakov, and J. Kim, J. Vac. Sci. Technol. A **31**, 050801 (2013).
[78]H. Y. Kim, J. Kim, L. Liu, C. F. Lo, F. Ren, and S. J. Pearton, J. Vac. Sci. Technol. B **31**, 051210 (2013).
[79]Y. L. Xi *et al.*, J. Vac. Sci. Technol. B **32**, 012201 (2014).
[80]X. Hu *et al.*, IEEE Trans. Nucl. Sci. **50**, 1791 (2003).
[81]J. Kim, F. Ren, D. Schoenfeld, S. J. Pearton, A. G. Baca, and R. D. Briggs, J. Semicond. Technol. Sci. **4**, 124 (2004).
[82]R. Khanna, K. K. Allums, C. R. Abernathy, S. J. Pearton, J. Kim, F. Ren, R. Dwivedi, T. N. Fogarty, and R. Wilkins, Appl. Phys. Lett. **85**, 3131 (2004).
[83]A. Y. Polyakov, N. B. Smirnov, A. V. Govorkov, A. V. Markov, S. J. Pearton, N. G. Kolin, D. I. Merkurisov, and V. M. Boiko, J. Appl. Phys. **98**, 033529 (2005).
[84]R. Khanna, S. Y. Han, S. J. Pearton, D. Schoenfeld, W. V. Schoenfeld, and F. Ren, Appl. Phys. Lett. **87**, 212107 (2005).
[85]A. Kalavagunta, A. Touboul, L. Shen, R. D. Schrimpf, R. A. Reed, D. M. Fleetwood, R. K. Jain, and U. K. Mishra, IEEE Trans. Nucl. Sci. **55**, 2106 (2008).
[86]A. Y. Polyakov, In-Hwan Lee, N. B. Smirnov, A. V. Govorkov, E. A. Kozhukhova, N. G. Kolin, A. V. Korulin, V. M. Boiko, and S. J. Pearton, J. Appl. Phys. **109**, 123703 (2011).
[87]Y.-H. Hwang *et al.*, J. Vac. Sci. Technol. B **32**, 031203 (2014).
[88]In-Hwan Lee, A. Y. Polyakov, N. B. Smirnov, A. V. Govorkov, E. A. Kozhukhova, N. G. Kolin, V. M. Boiko, A. V. Korulin, and S. J. Pearton, J. Vac. Sci. Technol. B **29**, 041201 (2011).
[89]A. P. Karmarkar, B. Jun, D. M. Fleetwood, R. D. Schrimpf, R. A. Weller, B. D. White, L. J. Brillson, and U. K. Mishra, IEEE Trans. Nucl. Sci. **51**, 3801 (2004).
[90]Xinwen Hu *et al.*, IEEE Trans. Nucl. Sci. **49**, 3213 (2002).
[91]Jian-Sian Li, Chao-Ching Chiang, Xinya Xia, Sergei Stepanoff, Aman Haque, Douglas E. Wolfe, Fan Ren, and S. J. Pearton, J. Appl. Phys. **133**, 015702 (2023).
[92]A. Yadav, E. Flitsiyan, L. Chernyak, Y. H. Hwang, Y. L. Hsieh, L. Lei, F. Ren, S. J. Pearton, and I. Lubomirsky, Radiat. Eff. Defects Solids **170**, 377 (2015).
[93]Chaker Fares, Fan Ren, Stephen J. Pearton, Gwangseok Yang, Jihyun Kim, Chien-Fong Lo, and J. Wayne Johnson, J. Vac. Sci. Technol. B **36**, 041203 (2018).
[94]F. Danesin, F. Zanon, S. Gerardin, F. Rampazzo, G. Meneghesso, E. Zanoni, and A. Paccagnella, Microelectron. Reliab. **46**, 1750 (2006).
[95]Keito Aoshima, Masahiro Horita, and Jun Suda, Appl. Phys. Lett. **122**, 012106 (2023).
[96]Edmund G. Seebauer and Meredith C. Kratzer, Mater. Sci. Eng. R. Rep. **55**, 57 (2006).
[97]D. Stievenard, Mater. Sci. Eng. B **71**, 120 (2000).
[98]J. Bourgoin and J. W. Corbett, Phys. Lett. A **38A**, 135 (1993).
[99]S. J. Pearton, J. C. Zolper, R. J. Shul, and F. Ren, J. Appl. Phys. **86**, 1 (1999).
[100]Matteo Meneghini *et al.*, J. Appl. Phys. **130**, 181101 (2021).
[101]A. Y. Polyakov *et al.*, J. Appl. Phys. **130**, 035701 (2021).
[102]A. Y. Polyakov *et al.*, J. Appl. Phys. **130**, 185701 (2021).
[103]M. A. J. Rasel, S. Stepanoff, A. Haque, D. E. Wolfe, F. Ren, and S. Pearton, Phys. Status Solidi RRL **16**, 2200171 (2022).
[104]Md Abu Jafar Rasel, Sergei P. Stepanoff, Maxwell Wetherington, Aman Haque, Douglas E. Wolfe, Fan Ren, and Stephen Pearton, Appl. Phys. Lett. **120**, 124101 (2022).
[105]Nahid Sultan Al-Mamun, Sergei Stepanoff, Aman Haque, Douglas E. Wolfe, Fan Ren, and Stephen Pearton, Appl. Phys. Lett. **121**, 233502 (2022).

07 April 2024 10:54:22

Published under an exclusive license by the AVS

[106]Md Abu Jafar Rasel, Sergei Stepanoff, Aman Haque, Douglas E. Wolfe, Fan Ren, and Stephen Pearton, ECS J. Solid State Sci. Technol. **11**, 075002 (2022).
[107]E. Mizuta, S. Kuboyama, Y. Nakada, A. Takeyama, T. Ohshima, Y. Iwata, and K. Suzuki, IEEE Trans. Nucl. Sci. **65**, 1956 (2018).
[108]B. D. Weaver, T. J. Anderson, A. D. Koehler, J. D. Greenlee, J. K. Hite, D. I. Shahin, F. J. Kub, and K. D. Hobart, ECS J. Solid State Sci. Technol. **5**, Q208 (2016).
[109]M. Zafrani, J. Brandt, R. Strittmatter, B. Sun, S. Zhang, and A. Lidow, *2022 IEEE Radiation Effects Data Workshop (REDW) (in Conjunction with 2022 NSREC)*, Provo, UT, 18–22 July 2022 (IEEE, 2022), pp. 1–4.
[110]S. A. Vitusevich, A. M. Kurakin, R. V. Konakova, A. E. Belyaev, and N. Klein, Appl. Surf. Sci. **255**, 784 (2008).
[111]Alexander Y. Polyakov *et al.*, J. Vac. Sci. Technol. B **30**, 041209 (2012).
[112]S. B. Witmer *et al.*, Mater. Sci. Eng., B **20**, 280 (1993).
[113]C. Sharma, A. K. Visvkarma, R. Laishram, A. Malik, K. Narang, S. Vinayak, and R. Singh, Semicond. Sci. Technol. **34**, 065024 (2019).
[114]M. P. Khanal, B. Ozden, K. Kim, S. Uprety, V. Mirkhani, K. Yapabandara, A. C. Ahyi, and M. Park, J. Vac. Sci. Technol. B **35**, 03D107 (2017).
[115]J. Lee, E. Flitsiyan, L. Chernyak, J. Salzman, and B. Meyler, ECS J. Solid State Sci. Technol. **6**, S3063 (2017).
[116]B. Luo *et al.*, Appl. Phys. Lett. **80**, 604 (2002).
[117]L. Scheick, IEEE Trans. Nucl. Sci. **61**, 2881 (2014).
[118]Przemysław Jozwik *et al.*, Phys. Chem. Chem. Phys. **24**, 25773 (2022).
[119]F. Moisy, M. Sall, C. Grygiel, A. Ribet, E. Balanzat, and I. Monnet, Nucl. Instrum. Methods Phys. Res., Sect. B **431**, 12 (2018).
[120]J. Gou, L. Q. Zhang, C. H. Zhang, Y. Song, Y. T. Yang, J. J. Li, Y. C. Meng, and H. X. Li, Nucl. Instrum. Methods Phys. Res., Sect. B **307**, 89 (2013).
[121]L. M. Zhang, W. Jiang, R. C. Fadanelli, W. S. Ai, J. X. Peng, T. S. Wang, and C. H. Zhang, Nucl. Instrum. Methods Phys. Res., Sect. B **388**, 30 (2016).
[122]Lu Liu *et al.*, J. Vac. Sci. Technol. B **31**, 022201 (2013).
[123]A. P. Karmarkar, B. D. White, D. Buttari, D. M. Fleetwood, R. D. Schrimpf, R. A. Weller, L. J. Brillson, and U. K. Mishra, IEEE Trans. Nucl. Sci. **52**, 2239 (2005).
[124]B. D. White, M. Bataiev, S. H. Goss, X. Hu, A. Karmarkar, D. M. Fleetwood, R. D. Schrimpf, W. J. Schaff, and L. J. Brillson, IEEE Trans. Nucl. Sci. **50**, 1934 (2003).
[125]H. Y. Kim, T. Anderson, M. A. Mastro, J. A. Freitas, Jr, S. W. Jang, J. Hite, C. R. Eddy, Jr, and J. Y. Kim, J. Cryst. Growth **326**, 62 (2011).
[126]H. Y. Kim, J. H. Kim, S. P. Yun, K. R. Kim, T. J. Anderson, F. Ren, and S. J. Pearton, J. Electrochem. Soc. **155**, H513 (2008).
[127]B. Luo *et al.*, Appl. Phys. Lett. **82**, 1428 (2003).
[128]G. Sonia *et al.*, Solid-State Electron. **52**, 1011 (2008).
[129]Byung-Jae Kim, Shihyun Ahn, Fan Ren, Stephen J. Pearton, Gwangseok Yang, and Jihyun Kim, J. Vac. Sci. Technol. B **34**, 041231 (2016).
[130]Shihyun Ahn, Byung-Jae Kim, Yi-Hsuan Lin, Fan Ren, Stephen J. Pearton, Gwangseok Yang, Jihyun Kim, and Ivan I. Kravchenko, J. Vac. Sci. Technol. B **34**, 051202 (2016).
[131]C. H. Li, H. L. Lu, Y. M. Zhang, M. Liu, and X. H. Zhao, IEEE Trans. Nucl. Sci. **62**, 1336 (2015).
[132]S. J. Cai *et al.*, IEEE Trans. Electron Devices **47**, 304 (2000).
[133]X. W. Hu *et al.*, IEEE Trans. Nucl. Sci. **50**, 1791 (2003).
[134]Amanda Portoff, Michael Stavola, W. Beall Fowler, Stephen J. Pearton, and Evan R. Glaser, Appl. Phys. Lett. **122**, 062101 (2023).
[135]F. C. Hila *et al.*, Radiat. Phys. Chem. **182**, 109331 (2021).
[136]J. Troska, S. Detraz, S. S. El Nasr-Storey, P. Stejskal, C. Sigaud, C. Soos, and F. Vasey, IEEE Trans. Nucl. Sci. **58**, 3103 (2011).
[137]A. H. Johnston, T. F. Miyahira, and B. G. Rax, IEEE Trans. Nucl. Sci. **48**, 1764 (2001).
[138]K. A. Gill, G. Cervelli, R. Grabit, F. B. Jensen, and F. Vasey, Proc. SPIE **4134**, 176.
[139]A. H. Johnston and T. F. Miyahira, IEEE Trans. Nucl. Sci. **51**, 3564 (2004).
[140]A. H. Johnston, IEEE Trans. Nucl. Sci. **50**, 689 (2003).
[141]Q. Du, Opt. Mater. Express **13**, 403 (2023).
[142]M. Osiński, P. Perlin, H. Sch€one, A. H. Paxton, and E. W. Taylor, Electron. Lett. **33**, 1252 (1997).
[143]F. Gaudreau, C. Carlone, A. Houdayer, and S. M. Khanna, IEEE Trans. Nucl. Sci. **48**, 1778 (2001).
[144]S. M. Khanna *et al.*, IEEE Trans. Nucl. Sci. **51**, 2729 (2004).
[145]Byung-Jae Kim, Ya-Hsi Hwang, Shihyun Ahn, Fan Ren, Stephen J. Pearton, Jihyun Kim, and Tae Sung Jang, J. Vac. Sci. Technol. B **33**, 051215 (2015).
[146]O. H. Pakarinen, F. Djurabekova, K. Nordlund, P. Kluth, and M. C. Ridgway, Nucl. Instrum. Methods Phys. Res., Sect. B **267**, 1456 (2009).
[147]M. Zerarka, P. Austin, A. Bensoussan, F. Morancho, and A. Durier, IEEE Trans. Nucl. Sci. **64**, 2242 (2017).
[148]C. Abbate, Microelectron. Reliab. **55**, 1496 (2015).
[149]Z. Islam, Angela L. Paoletta, Anthony M. Monterrosa, Jennifer D. Schuler, Timothy J. Rupert, Khalid Hattar, Nicholas Glavine, and Aman Haque, Microelectron. Reliab. **102**, 113493 (2019).
[150]A. Luchechko, V. Vasyltsiv, L. Kostyk, O. Tsvetkova, and A. I. Popov, Nucl. Instrum. Methods Phys. Res., Sect. B **441**, 12 (2019).
[151]S. Kuboyama, C. Kamezawa, N. Ikeda, T. Hirao, and H. Ohyama, IEEE Trans. Nucl. Sci. **53**, 3343 (2006).
[152]S. Kuboyama, C. Kamezawa, Y. Satoh, T. Hirao, and H. Ohyama, IEEE Trans. Nucl. Sci. **54**, 2379 (2007).
[153]S. Kuboyama, E. Mizuta, Y. Nakada, H. Shindou, A. Michez, J. Boch, F. Saigne, and A. Touboul, IEEE Trans. Nucl. Sci. **66**, 1688 (2019).
[154]T. Shoji, S. Nishida, K. Hamada, and H. Tadano, Jpn. J. Appl. Phys. **53**, 04EP03 (2014).
[155]H. Asai, K. Sugimoto, I. Nashiyama, Y. Iide, K. Shiba, M. Matsuda, and Y. Miyazaki, IEEE Trans. Nucl. Sci. **59**, 880 (2012).
[156]T. Makino, M. Deki, N. Iwamoto, S. Onoda, N. Hoshino, H. Tsuchida, T. Hirao, and T. Ohshima, IEEE Trans. Nucl. Sci. **60**, 2647 (2013).
[157]J.-M. Lauenstein, "Getting SiC power devices off the ground: Design, testing, and overcoming radiation threats," *Microelectronics Reliability and Qualification Working (MRQW) Meeting*, El Segundo, CA, February 2018; see: https://ntrs.nasa.gov/search.jsp?R=20180006113.
[158]S. S. Suvanam, L. Lanni, B. G. Malm, C. M. Zetterling, and A. Hallén, IEEE Trans. Nucl. Sci. **61**, 1772 (2014).
[159]M. Shakir, S. Hou, B. G. Malm, M. Östling, and C.-M. Zetterling, IEEE Electron Device Lett. **39**, 1540 (2018).
[160]P. G. Neudeck, D. J. Spry, L. Chen, N. F. Prokop, and M. J. Krasowski, IEEE Electron Device Lett. **38**, 1082 (2017).
[161]XinyXia, Nahid Sultan Al-Mamun, Daudi, Warywoba, Fan Ren, Aman Haque, and S. J. Pearton, J. Vacuum Sci. Technol. A **40**, 053403 (2022).
[162]T. Funaki, Juan Carlos Balda, Jeremy Junghans, Avinash S. Kashyap, H. Alan Mantooth, Fred Barlow, Tsunenobu Kimoto, and Takashi Hikihara, IEEE Trans. Power Electron. **22**, 1321 (2007).
[163]X. Jiang, K. Kim, S. Zhang, J. Johnson, and G. Salazar, Sensors **14**, 144 (2013).
[164]S. Roy *et al.*, IEEE Trans. Electron Devices **66**, 3764 (2019).
[165]P. Hazdra, V. Záhlava, and J. Vobecký, Solid State Phenom. **205-206**, 451 (2013).
[166]S. K. Dixit, S. Dhar, J. Rozen, S. Wang, R. D. Schrimpf, D. M. Fleetwood, S. T. Pantelides, J. R. Williams, and L. C. Feldman, IEEE Trans. Nucl. Sci. **53**, 3687 (2006).
[167]D. C. Sheridan, G. Chung, S. Clark, and J. D. Cressler, IEEE Trans. Nucl. Sci. **48**, 2229 (2001).
[168]A. Akturk, J. M. McGarrity, S. Potbhare, and N. Goldsman, IEEE Trans. Nucl. Sci. **59**, 3258 (2012).
[169]M. Nawaz, C. Zaring, S. Onoda, T. Ohshima, and M. Ostling, "Radiation hardness assessment of high voltage 4H-SiC BJTs," *2009 Device Research Conference, San Francisco, CA, 22-24 June 2009* (IEEE, New York, 2009), Vol. 6, pp. 279–280.
[170]J. N. Merrett *et al.*, Mater. Sci. Forum **483-485**, 885 (2005).

07 April 2024 10:54:22

Published under an exclusive license by the AVS

[171]C. Abbate, G. Busatto, D. Tedesco, A. Sanseverino, F. Velardi, J. Wyss, L. Silvestrin, F. Velardi, and J. Wyss, IEEE Trans. Electron Devices **66**, 4235 (2019).
[172]C. Abbate, G. Busatto, D. Tedesco, A. Sanseverino, F. Velardi, and J. Wyss, IEEE Trans. Electron Devices **66**, 4243 (2019).
[173]M. Usman and A. Hallén, IEEE Electron Device Lett. **32**, 1653 (2011).
[174]T. Ohshima, H. Itoh, and M. Yoshikawa, J. Appl. Phys. **90**, 3038 (2001).
[175]S. Onoda, N. Iwamoto, S. Ono, S. Katakami, M. Arai, K. Kawano, and T. Ohshima, IEEE Trans. Nucl. Sci. **56**, 3218 (2009).
[176]P. Peng Dong, Xiaolan Yan, Lin Zhang, Shangjie Jin, Fang Dai, Ying Zhang, Yingxin Cui, Xuegong Yu, and Bing Huang, IEEE Trans. Nucl. Sci. **68**, 312 (2021).
[177]R. Devanathan, W. J. Weber, and F. Gao, J. Appl. Phys. **90**, 2303 (2001).
[178]A. Khachatrian *et al.*, IEEE Trans. Nucl. Sci. **62**, 2743 (2015).
[179]A. Khachatrian *et al.*, IEEE Trans. Nucl. Sci. **66**, 368 (2019).
[180]Joel M. Hales *et al.*, IEEE Trans. Nucl. Sci. **67**, 81 (2020).
[181]Alexander Y. Polyakov *et al.* J. Appl. Phys. **132**, 035701 (2022).
[182]R. D. Harris, A. J. Frasca, and M. O. Patton, IEEE Trans. Nucl. Sci. **52**, 2408 (2005).
[183]K. Galloway *et al.*, Aerospace **5**, 67 (2018).
[184]D. R. Ball *et al.*, IEEE Trans. Nucl. Sci. **67**, 22 (2020).
[185]Arto Javanainen *et al.*, IEEE Trans. Nucl. Sci. **64**, 2031 (2017).
[186]A. Javanainen, K. F. Galloway, V. Ferlet-Cavrois, and J. M. Lauenstein, IEEE Trans. Device Mater. Reliab. **16**, 208 (2016).
[187]R. A. Johnson *et al.*, IEEE Trans. Nucl. Sci. **67**, 135 (2020).
[188]A. F. Witulski, R. Arslanbekov, A. Raman, R. D. Schrimpf, A. L. Sternberg, K. F. Galloway, Arto Javanainen, D. Grider, and D. J. Lichtenwalner, IEEE Trans. Nucl. Sci. **65**, 256 (2018).
[189]Pavel Hazdra, Petr Smrkovský, Jan Vobecký, and Andrei Mihaila, IEEE Trans. Electron Devices **68**, 202 (2021).
[190]A. Akturk, R. Wilkins, K. Gunthoti, S. A. Wender, and N. Goldsman, IEEE Trans. Nucl. Sci. **69**, 900 (2022).
[191]K. Niskanen, A. D. Touboul, R. Coq Germanicus, A. Michez, A. Javanainen, F. Wrobel, J. Boch, V. Pouget, and F. Saigné, IEEE Trans. Nucl. Sci. **67**, 1365 (2020).
[192]A. Titov, K. Karabeshkin, A. Struchkov, V. Nikolaev, A. Azarov, D. Gogova, and P. Karaseov, Vacuum **200**, 111005 (2022).
[193]D. R. Ball *et al.*, IEEE Trans. Nucl. Sci. **68**, 1430 (2021).
[194]Y. Nakada, S. Kuboyama, E. Mizuta, A. Takeyama, T. Ohshima, and H. Shindou, in *2019 19th European Conference on Radiation and Its Effects on Components and Systems (RADECS), Montpellier, France, 16-20 September 2019* (IEEE, New York, 2019), pp. 1–4.
[195]N. Ikeda, S. Kuboyama, Y. Satoh, and T. Tamura, IEEE Trans. Nucl. Sci. **55**, 3388 (2008).
[196]T. Shoji, S. Nishida, K. Hamada, and H. Tadano, Microelectron. Reliab. **55**, 1517 (2015).
[197]Manato Deki, Takahiro Makino, Naoya Iwamoto, Shinobu Onoda, Kazutoshi Kojima, Takuro Tomita, and Takeshi Ohshima, Nucl. Instrum. Methods Phys. Res., Sect. B **319**, 75 (2014).
[198]A. Akturk, J. M. McGarrity, N. Goldsman, D. J. Lichtenwalner, B. Hull, D. Grider, and R. Wilkins, IEEE Trans. Nucl. Sci. **66**, 1828 (2019).
[199]K. Niskanen, A. D. Touboul, R. C. Germanicus, A. Michez, A. Javanainen, F. Wrobel, J. Boch, V. Pouget, and F. Saigne, IEEE Trans. Nucl. Sci. **67**, 1365 (2020).
[200]A. Griffoni, J. Van Duivenbode, D. Linten, E. Simoen, P. Rech, L. Dilillo, F. Wrobel, P. Verbist, and G. Groeseneken, IEEE Trans. Nucl. Sci. **59**, 866 (2012).
[201]A. Javanainen *et al.*, IEEE Trans. Nucl. Sci. **64**, 415 (2017).
[202]A. Haran, J. Barak, D. David, N. Refaeli, B. E. Fischer, K. O. Voss, G. Du, and M. Heiss, IEEE Trans. Nucl. Sci. **54**, 2488 (2007).
[203]A. F. Witulski, Dennis R. Ball, Kenneth F. Galloway, Arto Javanainen, Jean-Marie Lauenstein, Andrew L. Sternberg, and Ronald D. Schrimpf, IEEE Trans. Nucl. Sci. **65**, 1951 (2018).
[204]A. Abbate, G. Busatto, S. Mattiazzo, A. Sanseverino, L. Silvestrin, D. Tedesco, and F. Velardi, Microelectron. Reliab. **88-90**, 941 (2018).
[205]C. Abbate, G. Busatto, P. Cova, N. Delmonte, F. Giuliani, F. Iannuzzo, A. Sanseverino, and F. Velardi, IEEE Trans. Nucl. Sci. **62**, 202 (2015).
[206]A. Akturk, J. M. McGarrity, N. Goldsman, D. J. Lichtenwalner, B. Hull, D. Grider, and R. Wilkins, IEEE Trans. Nucl. Sci. **65**, 1248 (2018).
[207]A. F. Witulski *et al.*, IEEE Trans. Nucl. Sci. **65**, 256 (2018).
[208]R. A. Johnson *et al.*, IEEE Trans. Nucl. Sci. **69**, 248 (2022).
[209]S. Liu *et al.*, IEEE Trans. Nucl. Sci. **59**, 1125 (2012).
[210]H. Asai, I. Nashiyama, K. Sugimoto, K. Shiba, Y. Sakaide, Y. Ishimaru, Y. Okazaki, K. Noguchi, and T. Morimura, IEEE Trans. Nucl. Sci. **61**, 3109 (2014).
[211]C. Martinella, R. Stark, T. Ziemann, R. G. Alia, Y. Kadi, U. Grossner, and A. Javanainen, IEEE Trans. Nucl. Sci. **66**, 1702 (2019).
[212]C. Martinella, T. Ziemann, R. Stark, A. Tsibizov, R. G. Alia, Y. Kadi, U. Grossner, and A. Javanainen, IEEE Trans. Nucl. Sci. **67**, 1381 (2020).
[213]C. Martinella, R. G. Alia, A. Coronetti, C. Cazzaniga, M. Kastriotou, Y. Kadi, R. Gaillard, U. Grossner, and A. Javanainen, IEEE Trans. Nucl. Sci. **68**, 634 (2021).
[214]Sethu Saveda Suvanam, "Radiation hardness of 4H-SiC devices and circuits," Ph.D. thesis in Information and Communication Technology (School of Information and Communication Technology, KTH Royal Institute of Technology, Stockholm, Sweden, 2017).
[215]C. Martinella, P. Natzke, R. G. Alia, Y. Kadi, M. Rossi, J. Jaatinen, H. Kettunen, U. Grossner, and A. Javanainen, Microelectron. Reliab. **128**, 114423 (2022).
[216]Corinna Martinella, "Single-event radiation effects in silicon carbide power MOSFETs," Dissertation (Department of Physics, University of Jyväskylä, Jyväskylä, Finland, 2021).
[217]P. Hazdra and J. Vobecky, Phys. Status Solidi A **216**, 1900312 (2019).
[218]P. F. Hinrichsen, A. J. Houdayer, A. L. Barry, and J. Vincent, IEEE Trans. Nucl. Sci. **45**, 2808 (1998).
[219]J. R. Srour, C. J. Marshall, and P. W. Marshall, IEEE Trans. Nucl. Sci. **50**, 653 (2003).
[220]G. P. Summers, E. A. Burke, C. J. Dale, E. A. Wolicki, P. W. Marshall, and M. A. Gehlhausen, IEEE Trans. Nucl. Sci. **34**, 1133 (1987).
[221]G. P. Summers, E. A. Burke, P. Shapiro, S. R. Messenger, and R. J. Walters, IEEE Trans. Nucl. Sci. **40**, 1372 (1993).
[222]J. R. Srour and D. H. Lo, IEEE Trans. Nucl. Sci. **47**, 2451 (2000).
[223]J. R. Srour and J. W. Palko, IEEE Trans. Nucl. Sci. **53**, 3610 (2006).
[224]P. Arnolda, C. Inguimbert, T. Nuns, and C. Boatella-Polo, IEEE Trans. Nucl. Sci. **58**, 756 (2011).
[225]F. El Allam, C. Inguimbert, A. Meulenberg, A. Jorio, and I. Zorkani, J. Appl. Phys. **123**, 095703 (2018).
[226]M. A. J. Rasel, S. Stepanoff, A. Haque, D. E. Wolfe, F. Ren, and S. J. Pearton, J. Vac. Sci. Technol. B **40**, 063204 (2022).
[227]J. Bourgoin, D. Peak, and J. W. Corbett, J. Appl. Phys. **44**, 3022 (1973).
[228]C. M. Zetterling, S. Kargarrazi, and M. Shakir, "Wide bandgap integrated circuits for high power management in extreme environments," in *Next-Generation ADCs, High-Performance Power Management, and Technology Considerations for Advanced Integrated Circuits*, edited by A. Baschirotto, P. Harpe, and K. Makinwa (Springer, Cham, 2020).

07 April 2024 10:54:22

Published under an exclusive license by the AVS